

Western  Graduate&PostdoctoralStudies

Western University
Scholarship@Western

Electronic Thesis and Dissertation Repository

2-25-2020 10:30 AM

Wave Propagation in Viscoelastic Dielectric Elastomer Media

Mohammad Mahdi Sheikh Bagher Mohajer
The University of Western Ontario

Supervisor
Jiang, Liying
The University of Western Ontario

Graduate Program in Mechanical and Materials Engineering
A thesis submitted in partial fulfillment of the requirements for the degree in Master of
Engineering Science
© Mohammad Mahdi Sheikh Bagher Mohajer 2020

Follow this and additional works at: <https://ir.lib.uwo.ca/etd>

Recommended Citation

Sheikh Bagher Mohajer, Mohammad Mahdi, "Wave Propagation in Viscoelastic Dielectric Elastomer Media" (2020). *Electronic Thesis and Dissertation Repository*. 6847.
<https://ir.lib.uwo.ca/etd/6847>

This Dissertation/Thesis is brought to you for free and open access by Scholarship@Western. It has been accepted for inclusion in Electronic Thesis and Dissertation Repository by an authorized administrator of Scholarship@Western. For more information, please contact wlsadmin@uwo.ca.

Abstract

Dielectric elastomers (DEs) are capable of producing large deformation under electric stimuli, which makes them desirable materials for a variety of applications including biomimetics, dynamics, robotics, energy harvesting, and waveguide devices. In general, DEs possess intrinsic hyperelasticity and viscosity. Such material properties may significantly affect the dynamic performance of DE-based devices. The delicate interplay among electromechanical coupling, large deformation, material viscosity and dynamics makes modeling of the performance of DE-based devices more challenging. Therefore, in order to provide guidelines for the optimal design of DE waveguide devices, it is essential to develop appropriate and reliable models, and efficient numerical methods to examine their performance first.

In this thesis, by integrating the state-of-art finite-deformation viscoelasticity theory into the framework of small-amplitude wave propagation superposed on a finitely deformed medium, the Rayleigh-Lamb wave propagation in a viscoelastic DE medium is investigated. Simulation results have demonstrated the effects of material viscosity, status of relaxation, external electric load, and mechanical pre-stretch on the dispersion behavior of the wave. For both pure elastic and viscoelastic DE media, waves with certain frequencies could be filtered by actively tuning electric loads. Moreover, some interesting findings conclude that the material viscoelasticity may cause some significant changes in the wave dispersion behavior. Therefore, incorporating the material viscosity in modeling DE waveguide is expected to provide more accurate prediction on their performance. This thesis will help to better understand the fundamentals of wave propagation in DE media and trigger more innovative and optimal design for DE waveguide applications.

Keywords: Rayleigh-Lamb wave; Electroelastic wave; Waveguide; Dielectric elastomers; viscoelasticity; hyperelasticity.

Summary for Lay Audience

Electroactive polymers (EAPs) are smart materials that exhibit unique mechanical response to an external electric field, which enables engineering designs to have more innovative features and functions. As one family of EAPs, dielectric elastomers (DEs) have received growing interest in soft material-based transduction technologies recently due to their large deformation capability, high energy density, softness and flexibility. In addition to the well-studied large-actuation and high-power applications for artificial muscles, soft robotics, biomimetics and energy harvesters, DE structures have also received attention for the dynamics applications as waveguide in recent years. The electromechanical coupling property of the material enables the DE waveguide to actively filter waves in the prescribed range of frequencies by adjusting the applied voltage.

In the literature, dynamic analysis on finitely deformed DEs is still very limited, particularly when involving material's intrinsic viscoelasticity. The lack of understanding the fundamentals underlying the electromechanical dynamics is certainly a major barrier for the full potential applications of DE waveguide. In order to overcome this obstacle, this thesis aims to establish a rigorous modeling and simulation framework to investigate the characteristics of wave propagation in dielectric media by adopting the finite-deformation viscoelasticity model for DEs. Simulation results will help to quantitatively understand the effects of material properties and electromechanical loads upon the wave propagation through DE media and how the waveguide can be tuned by the applied electrical stimuli. Thus, the fulfilment of this thesis is expected to provide better understanding of the fundamentals of wave propagation in DE media and be helpful for optimal design of DE waveguide.

Contents

Abstract	ii
Summary for Lay Audience	iii
List of Figures	vi
List of Tables	viii
1 Introduction	1
1.1 Rayleigh-Lamb wave propagation in elastic and viscoelastic solids	3
1.2 Dielectric elastomers, history, and applications	5
1.3 Objectives	7
1.4 Thesis structure	8
2 Literature Review	9
2.1 Dielectric elastomers in transduction technology applications	9
2.2 Hyperelastic constitutive models	16
2.3 Fully coupled field theory	19
2.4 Viscoelasticity	23
3 Rayleigh-Lamb wave propagation in a finitely deformed DE layer	30
3.1 Introduction	30
3.2 Problem Statement and Formulation	34
3.2.1 Finite-deformation viscoelasticity	36

3.2.2	Small amplitude fields superimposed on a finitely deformed DE	39
3.2.3	Wave propagation in a DE layer	42
3.3	Numerical Results and Discussion	46
3.4	Conclusions	61
4	Contributions, Conclusions, and Future Work	63
4.1	Thesis contributions and conclusions	63
4.2	Suggestions for future work	65
	Bibliography	66
	Curriculum Vitae	87

List of Figures

2.1	Schematic of a typical element of a dielectric elastomer transducer.	10
2.2	Dielectric elastomers designed with different configurations (Kornbluh et al., 2002).	11
2.3	Schematic of a dielectric body.	20
2.4	Schematic of Maxwell model.	24
2.5	Schematic of Kelvin-Voigt model.	25
2.6	Schematic of Standard linear model; a) Kelvin representation, b) Maxwell representation.	26
2.7	Schematic of Burgers model.	27
3.1	Schematics of an infinite DE layer (a) undeformed state, (b) deformed state . . .	35
3.2	Rheological model to illustrate the viscoelastic deformation of a DE layer . . .	35
3.3	variation of (a) $K(\hat{t})$ and (b) $G(\hat{t})$ with normalized time \hat{t}	47
3.4	Variation of normalized phase velocity with normalized wavenumber for an unstretched DE under different electrical loads. The continuous and dashed curves correspond to the symmetric mode and the antisymmetric mode, respectively. The scattered markers correspond to the results obtained by Shmuel et al. (2012) with filled and empty markers representing symmetric and antisymmetric modes, respectively.	48

3.5	Variation of normalized phase velocity with respect to normalized wavenumber for different values of $K(\hat{t})$ when (a) $\hat{d} = 0$, $\lambda = 1.5$ and $\chi = 0.8$, (b) $\hat{d} = 0$, $\lambda = 1.25$ and $\chi = 0.8$, and (c) $\hat{d} = 2$, $\lambda = 1.5$ and $\chi = 0.8$. The continuous and dashed curves correspond to the symmetric mode and the antisymmetric mode, respectively.	49
3.6	Variation of normalized group velocity with respect to normalized wavenumber for different values of $K(\hat{t})$ when (a) $\hat{d} = 0$, $\lambda = 1.5$ and $\chi = 0.8$, (b) $\hat{d} = 0$, $\lambda = 1.25$ and $\chi = 0.8$, and (c) $\hat{d} = 2$, $\lambda = 1.5$ and $\chi = 0.8$. The continuous and dashed curves correspond to the symmetric mode and the antisymmetric mode, respectively.	50
3.7	Variation of normalized phase velocity of (a) symmetric and (b) antisymmetric modes with normalized time when $\hat{d} = 0$, $\lambda = 1.5$, $\chi = 0.8$, and $K(0) = 0.7$	53
3.8	Variation of (a) normalized phase velocity \hat{c} and (b) normalized group velocity \hat{V}_G with normalized wavenumber \hat{k} for different material viscosity χ ($\lambda = 1.5$, $\hat{d} = 0$, and $K(\hat{t}) = 0.9$). The continuous and dashed curves correspond to the symmetric mode and the antisymmetric mode, respectively.	54
3.9	Effect of electrical load on the wave dispersion (a) normalized phase velocity, (b) normalized wave frequency, and (c) normalized group velocity for a pre-stretched viscous DE layer ($K(\hat{t}) = 0.9$, $\chi = 0.8$ and $\lambda = 1.5$). The continuous and dashed curves correspond to the symmetric mode and the antisymmetric mode, respectively.	57
3.10	Variation of (a) phase velocity and (b) group velocity with respect to pre-stretch ratio λ ($\hat{d} = 0.5$, $\chi = 0.8$, and $K(\hat{t}) = 0.9$).	57
3.11	Variation of (a) phase velocity and (b) group velocity with respect to electric displacement \hat{d} ($\lambda = 2$, $\chi = 0.8$, and $K(\hat{t}) = 0.9$).	59

List of Tables

3.1	Effect of (a) electric displacement \hat{d} and (b) pre-stretch λ on the particular wavenumber at which wave propagates independent of the relaxation status of the medium.	51
3.2	Effect of (a) material relaxation status $K(\hat{t})$, (b) normalized electric displacement \hat{d} , and (c) pre-stretch λ , on the critical value of material viscosity χ_{cr}	54
3.3	Effect of (a) material relaxation status $K(\hat{t})$, (b) material viscosity χ , and (c) pre-stretch λ , on the threshold of the electric displacement \hat{d}_{th}	58

Chapter 1

Introduction

Elastic wave refers to the oscillation of particles of matter while transferring energy through the media. The subject of wave propagation in elastic media has been studied for many decades. Unlike electromagnetic waves that may propagate in a vacuum as well as in a material medium, elastic waves need a transmission medium to exist. In general, elastic waves are categorized as longitudinal and transverse waves for which the energy is transferred, respectively, in the direction (or the opposite direction) and perpendicular to the direction of the motion of particles. Longitudinal elastic waves are alternatively called compression waves or pressure waves, while transverse elastic waves are also referred as shear waves. Depending on the amplitude of elastic waves with respect to the depth of the transmission medium, they can also be classified as body waves and surface waves. Body waves, which propagate through the interior of the medium, are further classified as primary waves (P-waves) and secondary waves (S-waves). P-waves, as a type of longitudinal waves, propagate faster than S-waves, a type of shear waves. On the other hand, surface waves are those propagating along the surface of a medium. Accordingly, the amplitude of the wave decays as they get further from the surface. Seismic waves in earthquakes consist of both body and surface waves. Although surface waves move slower than body waves, the seismic surface waves are more destructive during earthquakes.

The damage and the strength of the surface waves reduce in deeper earthquakes. Based on the motion of particles, surface waves are classified as Love waves and Rayleigh waves. Love waves, named after a British mathematician A.E.H. Love, have only one horizontal shear component motion of the particles. While Rayleigh waves have both longitudinal and transverse motions with amplitude decreasing exponentially as distance from the surface. Therefore, the motion of particles in Rayleigh waves is elliptical. Such surface waves are named after Lord Rayleigh, who predicted their existence in 1885 (Rayleigh, 1885). Distinct from these two types of surface waves, Lamb waves are a type of guided waves propagating through a layer medium, first analyzed by Horace Lamb (1917). The particle motion in this type of waves lies in the plane constructed by the wave propagation direction and the plane normal direction. In the literature, the term Rayleigh–Lamb waves embraces the Rayleigh wave. The motion of both Rayleigh and Lamb waves are constrained by the elastic properties of the surface(s) that guide them. The propagation of Rayleigh waves is guided by a single surface, while the Lamb wave is guided by two surfaces of the transmission medium.

Due to the capability of long distance propagation of Rayleigh and Lamb waves, they have been broadly studied and exploited in a wide range of applications including geophysics (Song et al., 1989; Beaty and Schmitt, 2003), seismology (Oliver, 1962), acoustics (Houmady et al., 1997; Vellekoop, 1998), telecommunications (Campbell, 1998; Morgan, 2010), and sensing and actuation (Lindner, 2008), among the others. Typically, the Lamb wave propagating through an elastic layer is decomposed into symmetric and antisymmetric modes with respect to the midplane of the plate medium (Lamb, 1917). Among different modes propagating through the layer, the two lowest ones have continuously attracted attention from researchers (Cho, 2000; Nicholson et al., 2002; Lee and Staszewski, 2003; Wan et al., 2016), which are called fundamental modes. This lies in two facts. One is that all the other Lamb wave modes have cut-off frequencies with the exception of these two lowest modes; while the other one is that the lowest modes carry more energy during the wave propagation. The funda-

mental symmetric mode (designated by S_0) is also called extensional mode, for which the plate is stretched in the direction of the propagation direction. On the other hand, the fundamental antisymmetric mode (designated by A_0) is also referred as flexural mode, for which the plate is bent as the two surfaces are disturbed to move in the same direction.

1.1 Rayleigh-Lamb wave propagation in elastic and viscoelastic solids

Elastic surface wave was named as Rayleigh wave after Lord [Rayleigh \(1885\)](#), who mathematically predicted its existence in compressible isotropic solids more than a century ago. This work was later extended to analyze and predict the characteristics of acoustic waves in elastic plates by Lord Rayleigh himself and [Lamb \(1917\)](#), which are named as Rayleigh-Lamb waves. In order to characterize the wave propagation in the elastic medium, the wave dispersion which relates the propagation velocity to the wave frequency or wavenumber must be determined ([Barnett and Lothe, 1985](#); [Pagneux and Maurel, 2001](#); [Galán and Abascal, 2002](#); [Gravenkamp et al., 2012a,b](#)). Generally, there are two types of velocity needs to be addressed. One is called phase velocity, at which the phase of wave propagates through the medium. The other one is group velocity, representing the rate at which the envelop shape of the waves combining various wavenumbers travels through the medium. However, the existence of Rayleigh-Lamb wave propagation was not observed in reality until [Worlton \(1961\)](#) provided experimental confirmation of Lamb waves at high frequencies. Since then Rayleigh-Lamb waves have been extensively used in waveguide devices. A comprehensive and detailed review on applications of surface elastic waves can be found in the work by [Alleyne \(1991\)](#). Among various applications of Rayleigh-Lamb wave propagation in elastic solids, non-destructive testing is a popular and practical technique in many engineering fields. For nondestructive testing, Rayleigh-Lamb waves are mainly used for two purposes. Firstly, the short distance wave propagation is used to

characterize material property of the object being tested (Chimenti and Nayfeh, 1990) and to detect existing defects close to interfaces (Xu and Bar-Cohen, 1990). For this case, the sensitivity in response to wave propagation is the key important criterion. The second purpose refers to large distance propagation used for inspection of large areas, including pipeline inspection (Ditri, 1994; Alleyen, 1997; Lowe et al., 1998) and inspection of defects in composites (Datta et al., 1990; Chimenti and Martin, 1991). For this application, noise to signal ratio and attenuation are two important factors for choosing a suitable Lamb wave mode. Attenuation mainly occurs due to the leakage of energy into surrounding fluid in any test structures containing fluid or being in contact with fluid. Hence the appropriate Lamb wave modes for this application are those having insignificant displacement at the contacting surface with the fluids. Usually the fundamental symmetric mode S_0 of Lamb waves at low frequency is the best fit to satisfy such criteria. Such a wave mode has low wave dispersion and the wave amplitude does not reduce as wave propagates through the medium. Therefore, the signal to noise ratio is constant along the way of propagation. Moreover, it has very low attenuation when the plate is in contact with a fluid.

In recent decades, rubber-like elastomeric materials have found a broad range of engineering applications, including medical devices (Leeper and Wright, 1983; Coury et al., 1988; McMillin, 1994; Modjarrad and Ebnesajjad, 2013), structural bearings and vibration isolators (Gueraud et al., 1985; Taylor et al., 1992; Kikuchi and Aiken, 1997; Kumar et al., 2014), sensors and actuators (Caldwell et al., 2000; Nguyen et al., 2004; Wissler and Mazza, 2007; Jung et al., 2008; Ohm et al., 2010; Ionov, 2014; Bilodeau et al., 2015) and so on. This is mainly due to their distinguished properties, such as lightweight, fracture tolerance, flexibility, easy manufacturability and low cost. Those elastomers exhibit hyperelasticity while are more or less viscous. Based on the change of strain rate with respect to stress, they are classified as linear and nonlinear viscoelastic materials. With the development of linear viscoelastic models, the problem of small-amplitude wave propagation in viscoelastic solids has attracted much

attention from the research community (Achenbach and Reddy, 1967; Tsai and Kolsky, 1968; Buchen, 1971; Sogabe and Tsuzuki, 1986; Carcione et al., 1988; Tal-Ezer et al., 1990). Particularly, the Rayleigh-Lamb wave propagation in linear viscoelastic solid has been well explored in the literature (Coquin, 1964; Romeo, 2001; Sharma, 2005; Sharma and Othman, 2007). Further progress in modeling the behavior of viscoelastic materials led to the incorporation of material nonlinearity for characterizing the wave propagation through viscoelastic plates. In this regard, some works were focused on analyzing small-amplitude wave propagation through finitely deformed layers (Hayes and Rivlin, 1969, 1972; Saccomandi, 2005; Destrade et al., 2009), while other studies were conducted to characterize finite-amplitude wave propagation through viscoelastic media (Hayes and Saccomandi, 2000, 2002; Destrade and Saccomandi, 2004, 2005). However, there is very limited study on the Rayleigh-Lamb wave propagation in nonlinear viscoelastic medium until a recent work (Mohabuth et al., 2019).

1.2 Dielectric elastomers, history, and applications

Recent advancements in the technology of polymeric materials have promoted their wide applications in industrial fields, such as automobiles, aerospace, household goods, electronics, and to name a few. Among various types of polymers, electroactive polymers (EAPs) are polymers that deform under electrical stimuli and convert electrical energy to mechanical energy in the meantime. Compared to electroactive ceramics such as the commonly used piezoelectric ceramics in traditional transduction technology with high load capacity, electroactive polymers are soft and capable of undergoing large deformation. Based upon the activation procedures, EAPs are classified as ionic EAPs and electronic EAPs. Ionic EAPs display their coupling effects due to mobility or diffusion of ions and their conjugated substances, while electronic EAPs deform subjected to electric field via the corresponding coulomb forces. Among a few types of electronic EAPs, dielectric elastomers (DEs) demonstrate softness, flexibility, light

weight, high energy density and large deformation capability. These distinguished properties extend promising applications of DEs in soft robots, artificial muscles, waveguide devices, adaptive optics, tactile sensors for Braille displays, and energy harvester scavenging energy from human walking and ocean waves (Pelrine et al., 2001; Brochu and Pei, 2010; Carpi et al., 2011; Kim et al., 2013; Park et al., 2014).

The electric field-induced deformation of a solid material was first observed by Alessandro Volta from the rupture of highly charged Leyden jar capacitors in 1776 (Carpi et al., 2010). One century later, the charge-induced deformation of a rubber band was reported by Rontgen (Keplinger et al., 2010). Following this experiment, Sacerdote (1899) conducted a research to capture the formulation of strain in response to an electric field activation. Eguchi (1925) discovered a piezoelectric polymer called electret when solidifying carnauba wax, rosin, and beeswax by cooling, which deformed when subjected to a DC bias electric field. Further milestone progress traces back nearly 20 years to a screening study by Pelrine et al. (1998) in which polyurethane, silicone, fluorsilicone, ethylene propylene, polybutadiene and isoprene were identified as dielectric materials capable of undergoing large deformation exhibiting surface strains up to 215%. This work marked the dawn of DEs, which has quickly attracted worldwide attention for the potential applications of DEs. Most efforts have been devoted to improving the actuation performance of DE actuators with different configurations (Pelrine and Kornbluh, 2000*a,b*), design and analysis on the energy harvesters (Pelrine et al., 2001; Chiba et al., 2008; Brochu et al., 2009; McKay et al., 2010; Kornbluh et al., 2012*b*; Huang et al., 2013; Shian et al., 2014), and DE-based devices and soft robots development (Kornbluh et al., 2002; Pei et al., 2004; Shian et al., 2015; Sun et al., 2016; Godaba et al., 2016; Duduta et al., 2017).

More recently, the concept of manipulating electroelastic waves and controlling band-gaps

by tuning an external electric field was initiated by [Gei et al. \(2010\)](#) through investigating small-amplitude flexural wave propagation through periodically actuated DE plate. Later, [Dorfmann and Ogden \(2010\)](#) adopted the quasi-electrostatic approximation to analyse small amplitude wave propagation through finitely deformed nonlinear electroelastic materials. This paper has been followed by a number of works on electroelastic wave propagation in finitely deformed homogenous and composite DEs ([Shmuel et al., 2012](#); [Shmuel and deBotton, 2012](#); [Shmuel, 2013](#); [Shmuel et al., 2013](#); [Galich and Rudykh, 2017](#)).

1.3 Objectives

As discussed in the previous sections, dielectric elastomers have demonstrated potentials in various engineering applications due to their unique features like flexibility, electromechanical coupling, high energy density, and particularly capability of sustaining large deformation. In contrast to the large body of research in the electroelastic statics of dielectric elastomers, the study of electroelastic dynamics is still at its infancy. This is mainly due to the complexity of the problems which involves the delicate interplay between electromechanical coupling, large deformation, material nonlinearity, and mechanical and electrical integrity. Although a few studies have been devoted to characterizing the wave propagation in elastomeric media, they are limited to either mechanical waves in viscoelastic media or electroelastic waves in pure hyperelastic media. To the best knowledge of the author, wave propagation through dielectric elastomers possessing both electromechanical coupling and material viscoelasticity has not been tackled yet in the literature. Therefore, the objective of this work is to develop a robust model and establish a framework for predicting the wave propagation through a finitely deformed dielectric medium as well as provide guidelines for the optimal design of active DE waveguides. In this regard, details are focused on:

- (1) Formulating the Rayleigh-Lamb wave propagation in a finitely deformed DE layer under

electromechanical loads with the incorporation of material viscoelasticity, and developing solution technique to derive wave dispersion relation;

- (2) Examining the effects of material viscosity as well electromechanical loads on the wave dispersion in a viscoelastic DE layer.

1.4 Thesis structure

Following the general introduction and objectives in Chapter 1, a detailed literature review about the relevant studies is given in Chapter 2, including the applications of dielectric elastomers, the hyperelasticity theories, the fully coupled field theory, and the finite-deformation viscoelastic models, and wave propagation. In Chapter 3, the formulation for the small-amplitude Rayleigh-Lamb wave propagation in a finitely deformed DE layer is derived based on the finite-deformation viscoelasticity theory for dielectric elastomers. Numerical solutions for case study are provided to investigate the effects of electromechanical loading as well as material viscosity on the wave dispersion relation. Finally, Chapter 4 summarizes the thesis and provides recommendations for future work.

Chapter 2

Literature Review

2.1 Dielectric elastomers in transduction technology applications

In recent years, dielectric elastomers (DEs) have been regarded as the most promising materials in soft-material-based electromechanical transduction technologies attributing to their unique properties. For example, DEs are characterized by their softness, flexibility and large deformation capability, ease of use, high coupling efficiency, light weight, cost effectiveness, high energy densities, and chemical and biological compatibility. Due to these distinguished properties for actuation, they have extensive potential applications, such as artificial muscles, adaptive optical elements, soft robots, programmable haptic surfaces, energy harvesters, active noise control devices, adaptive optical elements, and other biomimetic applications (Kornbluh et al., 2002; Pelrine et al., 2002; Heydt et al., 2006; O'Halloran et al., 2008; McKay et al., 2010; Carpi et al., 2011; Karsten et al., 2013; Huang et al., 2013).

The basic element of a DE transducer is a DE membrane coated with two compliant electrodes on its top and bottom surfaces as shown in Fig. 2.1. When the compliant electrodes are subject to a voltage V , opposite charges $\pm Q$ accumulate on the compliant electrodes. Then the attractive Maxwell force between the opposite charges makes the DE membrane reduce in thickness and expand in area. The strain induced by the applied electric field is expressed as,

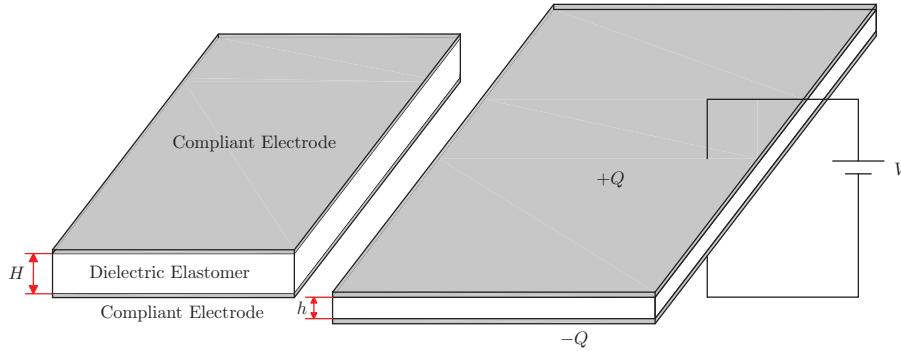


Figure 2.1: Schematic of a typical element of a dielectric elastomer transducer.

$$S = \frac{\epsilon_r \epsilon_0 V^2}{E h^2}, \quad (2.1)$$

where ϵ_0 is the permittivity of vacuum. In general, the response of the DE membrane depends on dielectric constant ϵ_r , mechanical stiffness E and electrical breakdown strength, i.e., the critical value of V/h with h being the thickness in the current state. Based on this basic element, the DE transducers could be designed with different configurations. Fig. 2.2 summarizes some typical configurations of transducers developed in the literature, ranging from simple beam structure to more complex spider shape for specific actuation tasks (Kornbluh et al., 2002). For example, the spider and bowtie, are designed to couple both planar directions into a single linear direction. Other configurations, such as the diaphragm, use both directions of deformation for actuation. The rolled configuration can create a large cross-sectional area of film for relatively high force applications. The framed actuator is designed for ease of manufacture, and it can be incorporated into essentially two-dimensional processes including MEMS techniques. These configurations of actuators have been implemented for the development of soft robots

and artificial muscles.

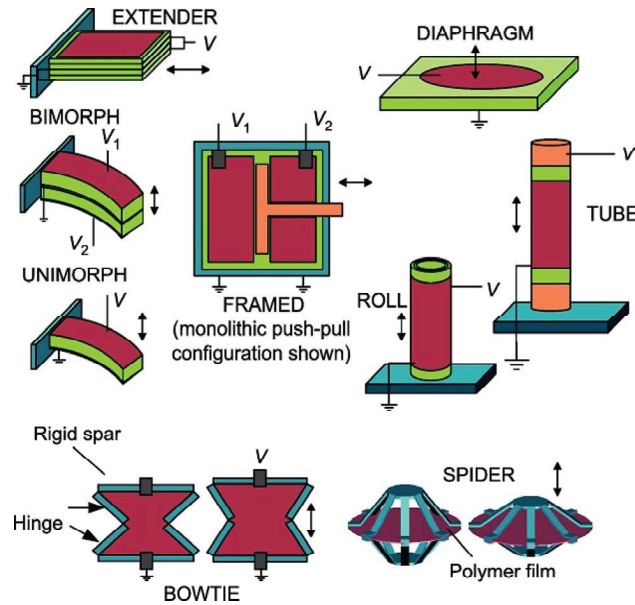


Figure 2.2: Dielectric elastomers designed with different configurations (Kornbluh et al., 2002).

As actuators, larger actuation is preferred. In the literature, it was found that a circular plate of DE can be strained up to 30% (Pelrine et al., 1998). In theory, it was predicted that giant deformation of actuation could be achievable if an elastomer follows a stress-stretch curve of a desirable form: the elastomer is compliant at small stretches and then stiffens steeply at modest stretches. Even 500% strain could be obtained theoretically (Kofod et al., 2003). However, the performance of DE actuators is mainly limited by electrical breakdown and saturation of electric field. To tackle this issue, better actuation performance under electrical load can be achieved by mechanical pre-stretching, adding interpenetrating networks in elastomers, or swelling elastomer with a solvent (Pelrine and Kornbluh, 2000a,b; Ha et al., 2006; Shankar et al., 2007; Zhu and Suo, 2010; Koh et al., 2011). Among various applications of DEs, they are very commonly used as artificial muscle or soft robots with the ability to resemble mechanical movements. Simple DE structures have been designed to provide gripper action or pick

and place function (Kofod et al., 2007). To improve the practicality of the DE grippers, multi-segment DE grippers consisting of repetitive DE segments with high aspect ratio was presented in 2014 (Araromi and Gavrilovich, 2014a,b). This design enables the gripper to wrap objects of various sizes. However, the grasping force of multi-segment DE grippers is not sufficient to hold up an object. Thus, in order to achieve a higher grasping capability, Heng et al. (2017) developed an arch-structured frame made of multi-segment DE grippers. Then, it was shown that pre-stretched multi-segment DE grippers has a higher bending moment resistance (Lau et al., 2017). More recently, novel strategies have been implemented to develop new design of DE grippers. In this regard, Shian et al. (2015) suggested a fiber-embedded DE gripper to restrict DE actuation in one direction and to induce bending in the perpendicular direction of the fibers. Furthermore, DE spring-roll bending actuators was introduced by Li and Liu (2019) to enhance the functionality of DE grippers. Pei et al. (2004) prototyped a six-leg robot to mimic the motion of cockroaches with six springs rolled by highly prestretched DE with patterned electrodes, which was actuated to move by the voltage-induced Maxwell stresses to bend the spring roll. A pivot roll bending DE actuator is designed to mimic the movement of a finger by Rosenthal and Pei (2008). Inspired by flying insects whose wings are driven indirectly by muscles, multi-staked actuators were used to develop flapping-wing vehicles (Lau et al., 2014). A jelly fish robot was presented by Godaba et al. (2016) with a DE balloon covered with a pre-stretched DE membrane. The voltage induced DE membrane expansion exerts a thrust force to lift the robot. More recently, with the use of laminated silicone layers and two DE actuators, a biomimetic robotic fish was designed to imitate the swimming of fish (Shintake et al., 2018). Another promising application of DEs is the development of focus tunable lens technology for the potential design of robotic systems, medical imaging devices, and optical detection tools. The adaptive focus tunable lenses are capable of tuning the focal length through changing either the refractive index of the optical medium or the shape of the lens surface profile. Recently, DE actuators with fast and highly reversible dynamic responses, low power consumption, mechanical robustness, and optical transparency are considered as appropriate tools to enhance

the functionality of adaptive focus tunable lenses. Inspired by human eyes, [Carpi and Frediani \(2011\)](#) suggested the implementation of DE actuators made of a transparent fluid between two DE membranes for the development of electrically tunable optical lenses and the model was further developed by [Shian et al. \(2013\)](#). Generally, in terms of the actuation mechanism, the DE adaptive focus tunable lenses are categorized into fluid-filled elastomeric lenses ([Carpi and Frediani, 2011](#); [Shian et al., 2013](#); [Wei et al., 2014](#); [Keong et al., 2014](#); [Rasti et al., 2015](#)), all-polymeric lenses ([Yun et al., 2015, 2016](#); [Nam et al., 2018](#); [Park et al., 2017](#)), and liquid droplet lenses ([Jin et al., 2016](#)).

Recently, DEs have also been developed as resonators or oscillators which are expected as a potential alternative to the traditional silicon-based devices in MEMS ([Zhang et al., 2005](#); [Bonwit et al., 2006](#); [Biggs and Hitchcock, 2010](#); [O'Brien et al., 2012](#)). The merit of a DE oscillator is that its natural frequency can be actively tuned by changing the applied voltage. Depending on specific applications, DE resonators are designed with different shapes, such as membrane and tube, on which most existing analyses for DE resonators and oscillators focus ([Mockensturm and Goulbourne, 2006](#); [Fox and Goulbourne, 2008, 2009](#); [Zhu et al., 2010a,b](#); [Yong et al., 2011](#); [Li et al., 2012](#); [Zhou et al., 2014, 2016b](#); [Li et al., 2019](#)). These DE oscillator modules can also be embedded in phones and tablets for haptic display as a facility to present information for people with vision or hearing impairments ([Carpi et al., 2009](#); [Möbinger et al., 2014](#); [Knoop and Rossiter, 2014](#); [Lee et al., 2014](#)).

Due to their high energy density and conversion efficiency, DEs are also considered for energy harvesting or generating from a various resources including human motions, ocean waves, and wind ([Lai et al., 2011](#); [Kornbluh et al., 2012a](#); [Chiba et al., 2013](#)). Usually DE generators are suitable for low-frequency application, ranging from 0.1 to 100 Hz, and are more applicable for large linear motion rather than rotary motion. A heel-strike generator with DE diaphragm

located in normal shoes or boots was designed by using the compression of the heel during normal walking as the means of harvesting power from human movement (Kornbluh et al., 2012b). DE power generators based on an articulated multibody system buoy at sea trial site have also been designed to harvest energy from ocean waves by stretching DE films (Brochu et al., 2009; Kornbluh et al., 2009). The energy harvesting mechanisms in those DE generators relies on the change of the capacitance of a DE membrane capacitor, which functions to collect and transfer electrical charges during an electromechanical loading process. Based on this harvesting mechanism, DE generators with various configurations and harvesting schemes have been developed in order to improve the energy harvesting performance (Pelrine et al., 2001; Chiba et al., 2008; Koh et al., 2009; McKay et al., 2010; Liu et al., 2010; Huang et al., 2013; Shian et al., 2014). Two exemplary energy harvesting schemes are the constant voltage one (Pelrine et al., 2001) and the triangular harvesting scheme (Shian et al., 2014). It should be noted that the development of energy harvesting schemes is also contingent on feasible implementation with electric circuits. Based on the finite-deformation viscoelasticity theory (Hong, 2011) and the nonlinear coupled field theory (Suo et al., 2008) for DEs, the energy harvesting performance of DE generators with both constant voltage and triangular harvesting schemes has been systematically investigated from the theoretical perspective by (Zhou et al., 2015, 2017). Their theoretical simulation results have proposed avenues to optimize the energy harvesting cycle of DE generators, which could significantly improve the energy harvesting performance of viscoelastic DE generators.

In the recent decades, active waveguide control has drawn attention from research community to investigate wave propagation in dielectric media. The concept of manipulating electroelastic waves and controlling band-gaps through tuning an external electric field was first presented by Gei et al. (2010) by studying the problem of small-amplitude flexural wave propagation in a periodically actuated DE plate. Later, Dorfmann and Ogden (2010) adopted the quasi-electrostatic approximation to analyze small-amplitude wave propagation through

finitely deformed electroelastic media. It was demonstrated in that work that the wave velocity could be significantly altered by any change in the applied electromechanical loads. Moreover, the effect of electromechanical coupling parameters on the wave velocity was also examined. The outcomes of these papers have stimulated a surge of scientific interests in electroelastic dynamics and consequently a series of works have been conducted to investigate the wave propagation in both homogeneous and inhomogeneous dielectric media. Based on the fully coupled field theory (Suo et al., 2008) and Neo-Hookean strain energy density function, Shmuel et al. (2012) investigated the Rayleigh-Lamb wave propagation through a finitely deformed elastic DE layer. It was demonstrated that both the wave velocities and frequencies were strongly affected by external electromechanical loads, which provides an avenue for actively filtering certain waves through applying electric field. Shmuel and deBotton (2012) studied the band-gap control through the small-amplitude wave propagation in a pre-stretched periodic laminate consisting of two layers of DEs. In this regard, the Bloch-Floquet theorem besides the transfer matrix method was implemented in order to obtain the corresponding dispersion relation. It was concluded that the band-gaps and filtered wave frequencies could be controlled via the phase properties and volume fraction, and most importantly the electric bias field. The results inspired Shmuel to investigate the problems of electroelastic wave propagation through a fiber-reinforced DE composites (Shmuel, 2013) and hollow DE cylinders (Shmuel et al., 2013) as well. It has demonstrated that properly tuning of the applied electric bias field could achieve the desirable properties of wave propagation in dielectric media. More recently, Galich and Rudykh (2017) studied the problem of shear wave propagation through compressible DE laminates, which reported that the applied electric bias field could have significant effect on both the phase and group velocities of shear wave. However, it has also shown that for dielectric medium governed by the Neo-Hookean model, the electric field has no influence on the shear wave band-gap.

Despite the numerous efforts in modeling the electroelastic statics of DEs and the recent

surge of interest in electroelastic dynamics, there is a knowledge gap in studying the wave propagation in dielectric media with the consideration of both material viscoelasticity and electromechanical coupling. It has thus motivated us to conduct a research regarding Rayleigh-Lamb wave propagation in a DE layer with the consideration of the above mentioned factors. In order to fulfill the full potential applications of DEs, we need to completely understand the delicate electromechanical coupling mechanisms of DEs. The following section provides a review on the relevant theories and models used to characterize the electromechanical coupling behavior of viscoelastic DEs.

2.2 Hyperelastic constitutive models

As well-established in the literature, DEs are capable of undergoing exceptionally large deformation with high nonlinearity. To capture the large deformation of DEs, hyperelastic constitutive models are commonly adopted. For the hyperelastic constitutive models, the stress-strain relationship of the material is obtained through a strain energy density function. Generally, hyperelastic models are developed based on three treatments, namely, the statistical mechanics treatments, the invariant-based continuum mechanics treatments and the stretch-based continuum mechanics treatments ([Boyce and Arruda, 2000](#)).

A detailed review on the statistical mechanics treatments for hyperelastic models can be found in the work by Treloar ([Treloar, 1975](#)), so that only the fundamental aspects will be revisited here. For the statistical mechanics treatments, it is assumed that rubber-like materials are formed by randomly-oriented long polymer chains. For the case that the elongation of polymer chains is significantly less than their fully extended length, the strain energy density

is captured by the Gaussian model as

$$W_G = \frac{1}{2}Nk\theta(\lambda_1^2 + \lambda_2^2 + \lambda_3^2), \quad (2.2)$$

where N is the number of chains, k is Boltzmann's constant, θ refers to the absolute temperature, λ_1 , λ_2 , and λ_3 are the principal stretch ratios. Nevertheless, when the elongation of the polymer chain is close to their extensibility, the results predicted by Gaussian model are quite different from the experimental results. Therefore, to consider the non-Gaussian nature of the polymer chains, other material models such as the three-chain model (Wang and Guth, 1952), the four-chain tetrahedral model (Flory and Rehner Jr, 1943), and the eight-chain model (Arruda and Boyce, 1993) have been developed. It is worth mentioning that for these models, the polymer is considered to have a representative network structure. For example, the eight-chain model assumes that the polymer chains rotate towards the principal axes of stretching and the corresponding strain energy density function is obtained as

$$W_{8ch} = Nk\theta \sqrt{n} \left[\beta_{chain} \lambda_{chain} + \sqrt{n} \ln \left(\frac{\beta_{chain}}{\sinh(\beta_{chain})} \right) \right], \quad (2.3a)$$

$$\lambda_{chain} = \sqrt{\frac{1}{3}(\lambda_1^2 + \lambda_2^2 + \lambda_3^2 - 3)}, \quad (2.3b)$$

$$\beta_{chain} = L^{-1} \left(\frac{\lambda_{chain}}{\sinh(\beta_{chain})} \right), \quad (2.3c)$$

where n designates the number of links in the chain and L^{-1} is the inverse Langevin function. It should be mentioned that although these non-Gaussian material models are capable of describing large deformation of the material, particularly when approaching to the material extensibility, they are inaccurate for small to moderate deformation.

On the other side, for the invariant-based continuum mechanics treatments, the strain

energy density function is given in terms of three invariants I_1 , I_2 , and I_3 defined as

$$I_1 = \lambda_1^2 + \lambda_2^2 + \lambda_3^2, \quad (2.4a)$$

$$I_2 = \lambda_1^2 \lambda_2^2 + \lambda_2^2 \lambda_3^2 + \lambda_3^2 \lambda_1^2, \quad (2.4b)$$

$$I_3 = \lambda_1^2 \lambda_2^2 \lambda_3^2. \quad (2.4c)$$

It should be noted that for an incompressible material, $\lambda_1 \lambda_2 \lambda_3 = 1$, leading to $I_3 = 1$. Rivlin (1948a) suggested a general form of strain energy density function based on these three invariants, i.e.,

$$W_R = \sum_{i,j=0}^{\infty} C_{ij} (I_1 - 3)^i (I_2 - 3)^j, \quad (2.5)$$

where C_{ij} are material constants. For the case that only invariant I_1 is preserved, this general model is reduced to the New-Hookean model with the strain energy density function defined as,

$$W_{NH} = C_{10} (I_1 - 3). \quad (2.6)$$

When only $(i, j) = (0, 1)$ as well as $(i, j) = (1, 0)$ are taken into account, the Mooney-Rivlin model (Mooney, 1940) is recovered as

$$W_{MR} = C_{10} (I_1 - 3) + C_{01} (I_2 - 3). \quad (2.7)$$

Furthermore, researchers have attempted to develop higher-order models in terms of the first invariant I_1 for describing moderate to large deformation. Yeoh model (Yeoh, 1993) can be mentioned as an example of these higher-order methods, which gives

$$W_Y = C_{10} (I_1 - 3) + C_{20} (I_1 - 3)^2 + C_{30} (I_1 - 3)^3. \quad (2.8)$$

However, none of invariant-based models mentioned above considers the extensibility of the polymer chains until Gent (1996) suggested a higher-order hyperelastic model to address this issue. According to the Gent model, the strain energy density function is given as

$$W_G = -\frac{GJ_{\text{lim}}}{2} \ln \left[\frac{1 - (I_1 - 3)}{J_{\text{lim}}} \right], \quad (2.9)$$

where G is the shear modulus of the material, and material parameter J_{lim} denotes the stretching limit of the material. Due to the existence of logarithmic function in Eq. (2.9), the inequality

$$\left[\frac{1 - (I_1 - 3)}{J_{\text{lim}}} \right] > 0, \quad (2.10)$$

must be satisfied and consequently the maximum stretch ratios are restricted by the value of J_{lim} .

On the other side, the stretch-based continuum mechanics treatment is another approach to construct the energy density function of hyperelastic materials. For this approach, the strain energy density function is expressed in terms of the principal stretch ratios, i.e., $W(\lambda_i)_{i=1,2,3}$. The Ogden model (Ogden, 1972) is one of the most common models in this class, which gives

$$W_{\text{O}} = \sum_n \frac{\mu_n}{\alpha_n} (\lambda_1^{\alpha_n} + \lambda_2^{\alpha_n} + \lambda_3^{\alpha_n}), \quad (2.11)$$

where μ_n and α_n are material constants. It should be noticed that the value of n in Eq. (2.11) can be adjusted to fit the experimental data.

2.3 Fully coupled field theory

As DEs are usually subjected to both mechanical and the electrical loads, the electromechanical coupling should be taken into account when describing their stress-strain relations. The demand for a robust constitutive model of DEs to characterize their electromechanical behavior has drawn continuous efforts. Inspired by the pioneering works of Toupin (1956), Eringen (1963), and Tiersten (1971), researchers have been prompted to formulate a field theory to capture the effect of the electrostatic force when analyzing the stresses of DEs (Pao, 1978; Eringen and Maugin, 1989; Maugin, 1992; Pelrine et al., 2000). Based on the assumption that the fields in the material can be separately calculated and added together to form the whole

field, these approaches have successfully explained some experimental phenomena. However, their physical origin still remains unclear and some of their predictions are inaccurate. Recent development in modelling of DEs has led to the development of fully coupled field theory (Dorfmann and Ogden, 2005; Suo et al., 2008), into which the hyperelastic models can be incorporated to capture the large deformation of DEs. This fully coupled field theory has been extensively employed by researchers to examine the electromechanical coupling behavior of DEs (Zhao and Suo, 2007, 2008; Zhou et al., 2008; Huang and Suo, 2011; Koh et al., 2011; Lu et al., 2012; Park et al., 2012). The fully coupled field theory developed by Suo et al. (2008) is briefly reviewed here.

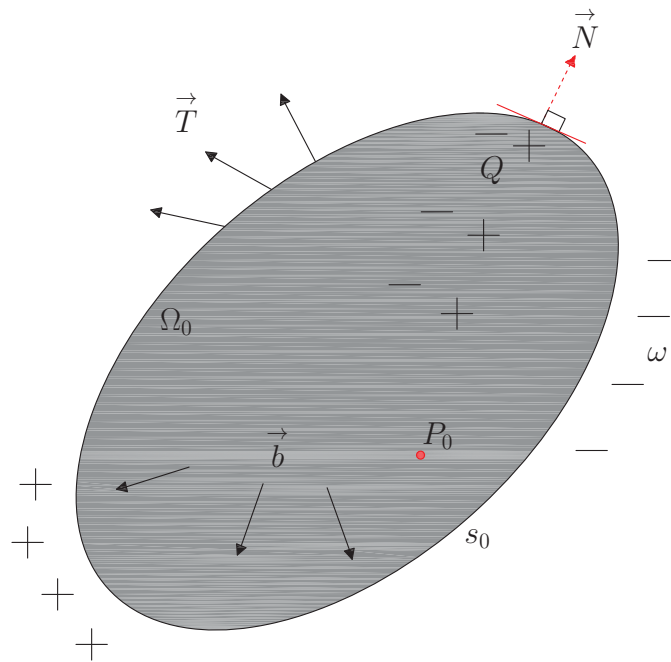


Figure 2.3: Schematic of a dielectric body.

Fig. 2.3 depicts a DE body with free body charge $Q(\mathbf{X}, t)$ and free surface charge $\omega(\mathbf{X}, t)$ subjected to body force $\mathbf{b}(\mathbf{X}, t)$, surface traction $\mathbf{T}(\mathbf{X}, t)$ and electric potential $\phi(\mathbf{X}, t)$. Also, the initial configuration of the DE body has a volume of Ω_0 , surface area of s_0 , and mass

density of ρ . Due to the electromechanical field applied on the DE body, a material particle P_0 moves from the reference position \mathbf{X} to the current position P with spatial coordinate $\mathbf{x}(\mathbf{X}, t)$ at time t . Hence the deformation gradient tensor \mathbf{F} of the current configuration with respect to the reference configuration is defined as

$$F_{ik} = \frac{\partial x_i(\mathbf{X}, t)}{\partial X_k}. \quad (2.12)$$

Satisfying the motion equations, the nominal stress (also called Piola Kirchhoff stress) S_{ik} satisfies the following equation,

$$\int_{\Omega_0} S_{ik} \frac{\partial \xi_i}{\partial X_k} d\Omega_0 = \int_{\Omega_0} \left(b_i - \rho \frac{\partial^2 x_i}{\partial t^2} \right) \xi_i d\Omega_0 + \int_{s_0} \xi_i T_i ds_0 \quad (2.13)$$

for any test function $\xi_i(\mathbf{X})$. As a special case, when the test function $\xi_i(\mathbf{X})$ takes the form of $\delta x_i(\mathbf{X}, \mathbf{t})$, the nominal stress S_{ik} is the work conjugate to the deformation gradient F_{ik} . Alternatively, for any small change of the deformation of the DE, the change in the strain energy density of the dielectric body is obtained as

$$\delta W^s = \int_{\Omega_0} S_{ik} \delta F_{ik} d\Omega_0. \quad (2.14)$$

Furthermore, the corresponding mechanical boundary condition yields,

$$(S_{ik}^- - S_{ik}^+) N_k = T_i, \quad (2.15)$$

where $N_k(\mathbf{X}, t)$ is the unit vector normal to the surface with "+" representing the direction pointing outward of the medium.

On the other hand, the nominal electric displacement \mathbf{D} satisfies the following equation

$$\int_{\Omega_0} -\frac{\partial \mu}{\partial X_k} D_k d\Omega_0 = \int_{\Omega_0} \mu Q d\Omega_0 + \int_{s_0} \mu \omega ds_0, \quad (2.16)$$

for any given scalar test function $\mu(\mathbf{X})$ when the Gauss's law is satisfied. It is worth mentioning that electric displacement is a vector field with the unit of coulombs per square metre (C/m^2),

which is equivalent to flux density in free space. Furthermore, the nominal electric field (\mathbf{E}) is given as

$$E_k = -\frac{\partial\phi}{\partial X_k}, \quad (2.17)$$

where ϕ is the electric potential. When μ takes the form of ϕ , for any small change of the volume charge δQ and the surface charges $\delta\omega$, the variation of the polarization energy W^p of the dielectric body can be expressed as

$$\delta W^p = \int_{\Omega_0} E_i \delta D_i. \quad (2.18)$$

Also, equation

$$(D_k^+ - D_k^-) N_k = \omega, \quad (2.19)$$

must be satisfied according to the electric boundary conditions at the surface of the dielectric body.

Let W be the Helmholtz free energy density of the dielectric body and δW be its change associated with the displacement and charge redistribution. According to Eqs. (2.14) and (2.18), the corresponding change in the total free energy of the system, G , takes the form of

$$\delta G = \int_{\Omega_0} (\delta W - S_{ik} \delta F_{ik} - E_k \delta D_k) d\Omega_0. \quad (2.20)$$

Complying with the second law of thermodynamics, the total free energy of the system never increases, i.e., $\delta G \leq 0$. Hence the inequality

$$\delta W - S_{ik} \delta F_{ik} - E_k \delta D_k \leq 0, \quad (2.21)$$

must be satisfied for any considered volume of the dielectric body. The equal sign holds true only for reversible processes. For pure elastic DEs,

$$\delta W = \frac{\partial W}{\partial F_{ik}} \delta F_{ik} + \frac{\partial W}{\partial D_k} \delta D_k. \quad (2.22)$$

Thus, the constitutive equations for a pure elastic DE medium according to the fully coupled field theory are obtained as

$$S_{ik} = \frac{\partial W(\mathbf{F}, \mathbf{D})}{\partial F_{ik}}, \quad (2.23a)$$

$$E_k = \frac{\partial W(\mathbf{F}, \mathbf{D})}{\partial D_k}. \quad (2.23b)$$

Accordingly, the true stress $\boldsymbol{\sigma}$, the true electric displacement \mathbf{d} , and the true electric field \mathbf{e} can be determined in terms of the corresponding nominal quantities, i.e.,

$$\sigma_{ij} = \frac{S_{ik} F_{jk}}{\det(\mathbf{F})}, \quad (2.24a)$$

$$d_i = \frac{D_k F_{ik}}{\det(\mathbf{F})}, \quad (2.24b)$$

$$e_i = F_{ik}^{-1} E_k. \quad (2.24c)$$

In addition, experiments suggest

$$d_i = \varepsilon_0 \varepsilon_r e_i, \quad (2.25)$$

where ε_0 and ε_r are, respectively, the permittivity of the vacuum and the relative dielectric constant of the DE medium.

2.4 Viscoelasticity

As well-established in the literature, most DEs are possess viscoelasticity. Material viscosity allows DEs to dissipate energy during the deformation. A typical stress-strain curve for viscoelastic materials demonstrates a hysteresis loop with the area within the loop representing the dissipated energy. Generally, rheological models such as the Maxwell model, the Kelvin-Voigt model and the Burger's model can be used to describe the viscoelastic nature of the material.

- **Maxwell model**

As shown in Fig. 2.4 , the Maxwell model is formed by an elastic spring and a purely viscous damper, which are connected in series. It can be noted that once the material is stretched, the whole deformation is immediately sustained by the elastic spring while the viscous element remains unchanged. Then the deformation in the viscous element increases with time while the spring relaxes, leading to a decrease of the stress. Therefore, the total strain can be obtained by adding the strain of elastic and viscous elements together, i.e.,

$$\varepsilon = \varepsilon_e + \varepsilon_v, \quad (2.26a)$$

$$\varepsilon_e = \frac{\sigma}{E}, \quad (2.26b)$$

$$\varepsilon_v = \frac{\dot{\sigma}}{\eta}, \quad (2.26c)$$

where ε , ε_e , and ε_v represent the total, the elastic, and the inelastic strain, respectively; σ is the stress; E is the elastic modulus of the spring, η is the viscosity of the material, and the over-dot quantity denotes the differentiation of the quantity with respect to time. According to Eq. (2.26), the constitutive equation for the Maxwell model is derived as

$$\sigma + \frac{\eta}{E} \dot{\sigma} = \eta \dot{\varepsilon}. \quad (2.27)$$

With the constitutive equation (2.27), the Maxwell model is capable of capturing the stress relaxation of materials, while cannot predict the creep of polymers.



Figure 2.4: Schematic of Maxwell model.

- **Kelvin-Voigt model**

The elastic and viscous elements in Kelvin-Voigt model are connected in parallel as shown in Fig. 2.5. Therefore, the strain in the spring is always the same as that in the viscous element.

Therefore, the constitutive equation according to the Kelvin-Voigt model is written as

$$\sigma = E\varepsilon + \eta\dot{\varepsilon}, \quad (2.28a)$$

$$\varepsilon = \varepsilon_e = \varepsilon_v. \quad (2.28b)$$

In contrast to the Maxwell model, upon application of a constant stress the Voigt model predicts that the strain rate decreases with time, making it appropriate to explain the creep characteristics of polymers.

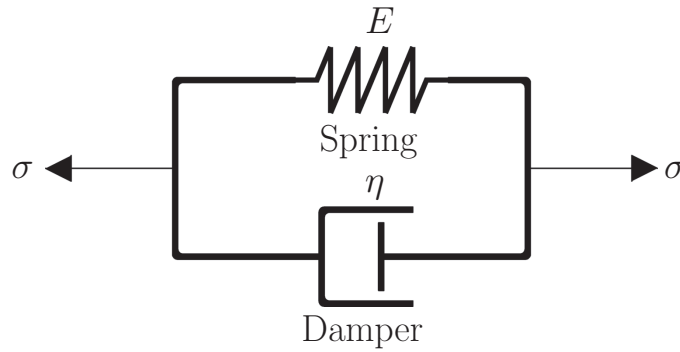


Figure 2.5: Schematic of Kelvin-Voigt model.

- **Standard linear solid model**

The standard linear solid model is formed by two springs and one dashpot. The elements can be arranged as either a Maxwell element being in parallel with an elastic spring or an elastic spring being in series with a Voigt element. Figs. 2.6a and 2.6b depict, respectively, the Kelvin and Maxwell representation of the standard linear model. These are the simplest arrangements of springs and dashpots that can work properly to predict both the relaxation and the creep behaviors of polymers. The constitutive equation with regard to the Maxwell representation takes the form of

$$\sigma + \frac{\eta}{E_2}\dot{\sigma} = E_1\varepsilon + \frac{\eta(E_1 + E_2)}{E_2}\dot{\varepsilon}, \quad (2.29)$$

where E_1 and E_2 are the elastic moduli of the elastic spring and the Maxwell element, respectively. On the other hand, the constitutive equation with the Kelvin representation is given

as

$$\sigma + \frac{\eta}{E_1 + E_2} \dot{\sigma} = \frac{E_1 E_2}{E_1 + E_2} \varepsilon + \frac{E_1 \eta}{E_1 + E_2} \dot{\varepsilon}, \quad (2.30)$$

where E_1 and E_2 are the elastic moduli of the elastic spring and the Voigt spring, respectively. By considering the constitutive equations, it can be noted that under a constant stress, both representations of the Standard linear solid model undergo some instantaneously deformation, then the deformation gradually increases and asymptotically approaches to a steady-state strain.

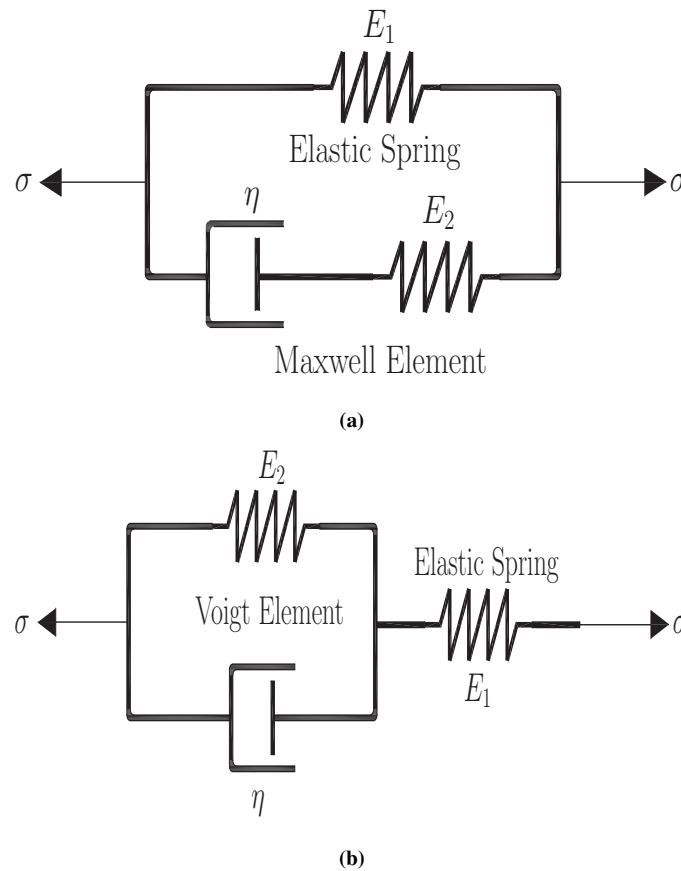


Figure 2.6: Schematic of Standard linear model; a) Kelvin representation, b) Maxwell representation.

- **Burgers model**

Fig. 2.7 demonstrates the schematic of the Burgers model, which is formed by a Maxwell element and a Voigt element in series. Therefore, the corresponding constitutive equation is

$$\sigma + \left(\frac{\eta_1}{E_1} + \frac{\eta_2}{E_1} + \frac{\eta_2}{E_2} \right) \dot{\sigma} + \frac{\eta_1 \eta_2}{E_1 E_2} \ddot{\sigma} = \eta_2 \dot{\epsilon} + \frac{\eta_1 \eta_2}{E_1} \ddot{\epsilon}, \quad (2.31)$$

where E_1 and E_2 represents the elastic moduli of the spring in the Voigt and the Maxwell elements, respectively; η_1 and η_2 are the viscosity of Voigt and Kelvin elements, respectively. From the constitutive equation (2.31), it can be noted that, subjected to a constant load, the strain continuously increases and asymptotically approaches to a steady-state strain.

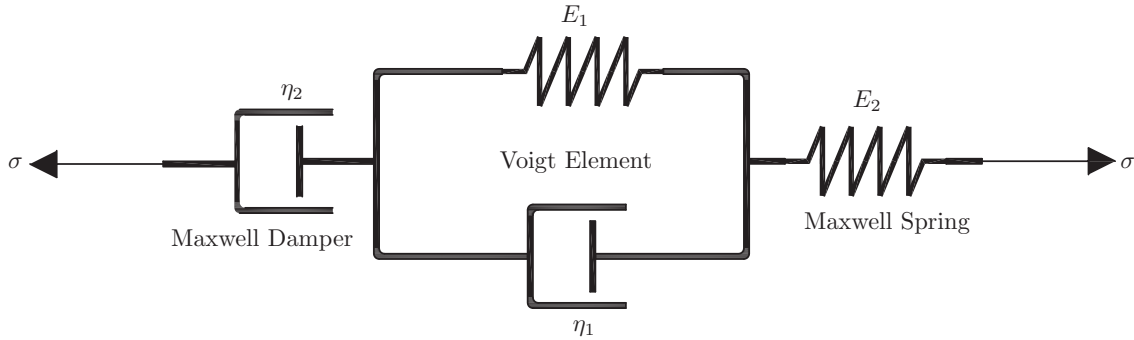


Figure 2.7: Schematic of Burgers model.

• Finite-deformation viscoelasticity models

When considering finite deformation of the material, the deformation of the springs in the above mentioned rheological models is nonlinear, which is often the case for rubber-like materials elastomers. Generally, there are two major approaches to model the finite-deformation viscoelasticity of elastomers. One is the hereditary integral method that utilizes fading-memory functions to reflect the strain history on the current stress-state (Simo, 1987; Drozdov, 1997; Kaliske and Rothert, 1997). The other approach is based on the multiplicative decomposition of the deformation gradient into an elastic and an inelastic part, i.e.,

$$\mathbf{F} = \mathbf{F}^e \mathbf{F}^i, \quad (2.32)$$

where \mathbf{F} , \mathbf{F}^e , and \mathbf{F}^i denotes the total, the elastic and the inelastic deformation gradient tensors, respectively. The framework of this approach was initiated by [Green and Tobolsky \(1946\)](#) and further exploited by other researchers with the incorporation of certain hyperelastic models to represent the energy density of the springs ([Sidoroff, 1982](#); [Reese and Govindjee, 1998](#); [Bergström and Boyce, 2000](#); [Reese, 2003](#)).

In the literature, it has long been realized that the viscoelastic properties and the rate-dependent deformation of elastomers can significantly affect the performance of DE-based devices ([Pelrine and Kornbluh, 2000a](#); [Löwe et al., 2005](#); [Plante and Dubowsky, 2006](#); [Wissler and Mazza, 2007](#)). Therefore, modeling the finite-deformation viscoelasticity of DEs is essential for predicting the electromechanical behavior of DE-based devices. In fact, substantial efforts have been devoted to tackling this issue for DEs. The early study can be traced back to a work done by [Christensen \(1980\)](#), which examined the creep of viscoelastic elastomers. Following the same framework, [Yang et al. \(2005\)](#) developed a nonlinear viscoelastic model for DEs. [Wissler and Mazza \(2005\)](#) presented a quasi-linear viscoelastic model to study the time-dependent response of a circular DE membrane. Later, [Plante and Dubowsky \(2007\)](#) proposed a modified hyperelasticity theory to address the finite-deformation viscoelasticity of DEs and examine their dynamic performance. However, these works are either limited to relatively small deformations or only successful to capture some finite-deformation experimental phenomena. Recently, combining the finite-deformation viscoelasticity theory by [Reese and Govindjee \(1998\)](#) and the fully coupled field theory by [Suo et al. \(2008\)](#), [Hong \(2011\)](#) presented a model that can account for viscoelastic effect on the electromechanical coupling of DEs. The model by Hong is capable of adopting most hyperelastic constitutive models and the evolution laws for viscoelastic solids. Adopting the Maxwell representation of the standard solid rheological model, the strain energy of Hong's model is split into two parts, i.e., the strain energy density stored in elastic spring and the strain energy stored in the Maxwell element. The more detailed information of this framework is elaborated in Chapter 3. The Hong's model was

further employed by Wang et al. ([Wang, Lei and Cai, 2013](#)) who examined the inhomogeneous deformation of a viscoelastic DE membrane. Moreover, with the same modeling framework, it is also found that the dynamic and the energy harvesting performance of the DEs can be strongly affected by their material viscoelasticity ([Foo et al., 2012](#); [Sheng et al., 2013](#); [Liu, 2014](#); [Shian et al., 2014](#); [Zhou et al., 2015, 2016a,b, 2017](#); [Li et al., 2019](#)).

Chapter 3

Rayleigh-Lamb wave propagation in a finitely deformed DE layer

3.1 Introduction

Dielectric elastomers (DEs), capable of producing large strains under electric stimuli, exhibit exceptional potentials for a variety of applications such as artificial muscles, soft robots, energy harvesters, adaptive optics, tactile sensors for Braille displays, and tunable waveguide (Pelrine et al., 2001; Brochu and Pei, 2010; Carpi et al., 2011; Kim et al., 2013; Park et al., 2014). DE waveguide, which offers an alternative to manipulating elastic waves via the application of an electric field to the DE medium, has attracted much interest in recent decades (Hensel and Gillings, 1986; Shmuel et al., 2013; Galich and Rudykh, 2016; Ziser and Shmuel, 2017). Although the potential applications of DE waveguide are very promising, predicting their performance is still very challenging due to the complexity of the problem with the involvement of large deformation, electromechanical coupling, and especially material viscoelasticity of DEs. Therefore, this work aims to tackle this challenge by developing a comprehensive model to in-

investigate the characteristics of wave propagation in a DE layer with the consideration of these factors.

For most DE applications, they are usually subjected to coupled electromechanical loads and undergo large deformations. An appropriate constitutive model that accounts for both electromechanical coupling and finite deformation is thus required, which has drawn continuous efforts in the research community. Inspired by the pioneering works (Toupin, 1956; Eringen, 1963; Tiersten, 1971), researchers have been prompted to formulate constitutive laws to capture the effect of electrostatic loads when analyzing the deformation of DEs (Pao, 1978; Eringen and Maugin, 1989; Maugin, 1992; Pelrine et al., 2000). By adding the effect of Maxwell force on the mechanical deformation directly, these studies have successfully explained some experimental phenomena. However, the physical origin of these experimental phenomena remains unclear and some of their predictions are inaccurate particularly when DEs are subjected to large deformation. Recently, with the development of fully coupled field theories (Dorfmann and Ogden, 2005; Suo et al., 2008), various hyperelastic models (Rivlin, 1948a,b; Ogden, 1972; Yeoh, 1993; Gent, 1996) have been incorporated to establish the constitutive relations for investigating the electromechanical coupling behavior of DEs with the consideration of their finite deformations. For example, Zhao et al. (2007) studied the electromechanical instability and co-existent states of DEs. Huang and Suo (2011) demonstrated that the electromechanical energy conversion can be significantly improved by utilizing the phase transition of DEs with a particular combination of material properties. Koh et al. (2011) explored possible mechanisms to achieve large actuation strain in DEs. Lu et al. (2012) investigated the electromechanical deformation of fiber-reinforced DEs under different loading conditions. The coupled field theories have also laid a foundation for finite element simulation of the electromechanical coupling of DEs in later studies (Zhao and Suo, 2008; Zhou et al., 2008; Park et al., 2012).

Moreover, it has long been recognized that DEs are more or less viscous (Pelrine and Ko-

rnbluh, 2000a; Löwe et al., 2005; Plante and Dubowsky, 2006), which strongly influences their electromechanical coupling behavior. For example, it is found that the material viscosity has significant effects on the frequency tuning and the dynamic performance of DE-based devices (Zhang et al., 2004; Plante and Dubowsky, 2007; Bai et al., 2014; Kollosche et al., 2015). In fact, predicting the time-dependent and viscoelastic behaviors of DEs has received much attention since the last decade. Some early works focused on theories of linear viscoelasticity to model relatively small deformations of DEs (Yang et al., 2005; Wissler and Mazza, 2005; Plante and Dubowsky, 2007). These models either only considered the mechanical behavior of DEs or formulated the electromechanical coupling by simply adding the Maxwell stress. Later, Wissler and Mazza (2007) presented a quasi-linear viscoelastic model in which Prony series were introduced into the strain energy function to capture the material's time-dependent properties. Wang, Xue, Chen and Qiang (2013) developed a constitutive relation for DEs based on the Kelvin-Voigt rheological model to characterize their energy dissipation under uniaxial stretching and loading-unloading cycles. Recently, Hong (2011) has developed a finite-deformation viscoelasticity theory for DEs which is capable of capturing both the finite inelastic deformation and the electromechanical coupling of DEs. The merit of this model lies in the fact that it provides a theoretical framework capable of adopting most finite-deformation constitutive models and thermodynamics evolution laws for viscoelastic solids. Based on this rigorous model, the frequency tuning of DE-based oscillators and energy harvesting performance of DE generators have been well explored (Zhou et al., 2014, 2017; Zhang et al., 2015).

In contrast with the large body of theoretical and modeling works on the static behavior of DEs, the study on wave propagation in a DE medium is relatively limited. The concept of manipulating electroelastic waves and controlling band-gaps by electric bias field was first proposed by Gei et al. (2010) via investigating small-amplitude flexural wave propagation through a periodically actuated DE plate. Considering quasi-electrostatic finite deformation and small-amplitude wave propagation, the pioneering work by Dorfmann and Ogden (2010) has laid

a foundation and established a framework for later studies on DE waveguide. Adopting the neo-Hookean model to describe the finite deformation, [Shmuel et al. \(2012\)](#) investigated the Rayleigh-Lamb wave propagation through a finitely deformed DE layer. It was demonstrated that the wave dispersion relations were strongly affected by the electrical load as well as the pre-stretching of the DE layer, leading to a conclusion that waves with certain frequencies could be filtered by applying a suitable electric field to the DE medium. Following this work, Shmuel has conducted a series of studies on the wave propagation problems. For example, [Shmuel and deBotton \(2012\)](#) investigated the thickness vibration of a finitely deformed periodic DE laminate by using the Bloch-Floquet theorem and the transfer matrix method. Their simulation results demonstrated how the band-gaps could be actively modified by the electric bias field. The dependence of band structures of fiber-reinforced DE composites on the phase properties and volume fraction, and most importantly the bias electric field has also been evaluated by [Shmuel \(2013\)](#). The results suggest the use of DE composites to control electroelastic wave propagation by properly tuning the electric bias field. Later the axisymmetric wave propagation through hollow DE cylinders was studied by [Shmuel et al. \(2013\)](#). The influences of the tube geometry, the mechanical pre-stretch and the electric bias field on the wave dispersion infer the use of DE in tubular configurations as tunable waveguide by electric stimuli. [Galich and Rudykh \(2017\)](#) investigated the wave propagation through compressible DE laminates, demonstrating the possible manipulation of wave band-gaps through the electric field.

It should be mentioned that in the current literature the intrinsic material viscosity possessed by most DEs has been ignored in studying the wave propagation in a DE medium, which may result in substantial error when characterizing the wave dispersion relation. Therefore, the material viscosity of DEs is a significant issue needs to be tackled for DE waveguide. In this study, based on the theory of finite-deformation viscoelasticity ([Hong, 2011](#)), the Rayleigh-Lamb wave propagation through a finitely deformed DE layer with the consideration of material viscoelasticity is investigated. Following the work by [Dorfmann and Ogden](#)

(2010), the equations of motion are obtained by considering an incremental time-dependent motion field superimposed on the finitely deformed DE layer. Numerical results will illustrate the effects of the mechanical pre-stretch, the applied electric field, and the material viscoelasticity on the dispersion relation, which is expected to provide a better understanding on the waveguide control through the use of viscoelastic DEs.

3.2 Problem Statement and Formulation

In this study, we will focus on the Rayleigh-Lamb wave propagation in a finitely deformed viscoelastic dielectric elastomer (DE) layer as described by a Cartesian coordinate system $x_1x_2x_3$ in Fig. 3.1a. The layer is infinitely long along the x_1 -axis with an initial thickness $2H$ along the x_2 -axis direction in the undeformed or the reference state. The DE layer is coated with compliant electrodes on its top and bottom surfaces, which are traction free. The DE layer is first pre-stretched along the x_1 -axis direction with a stretch ratio λ and then the stretch ratio is fixed by clamping the DE layer. Subsequently, an electric displacement d is applied in the thickness direction, which reduces the tension or induces compression in the x_1 -direction in the DE layer. Fig. 3.1b shows the deformed state of the DE layer with thickness $2h$, also referred as the current state. Assuming the plane-strain condition for the current study, there is no deformation along the x_3 -axis and consequently the fields are independent of x_3 . Under the homogeneous deformation assumption, the deformation gradient of the current state with

respect to the undeformed state can be expressed as $\mathbf{F} = \begin{bmatrix} \lambda & 0 & 0 \\ 0 & \lambda_h & 0 \\ 0 & 0 & 1 \end{bmatrix}$ with $\lambda_h = h/H$.

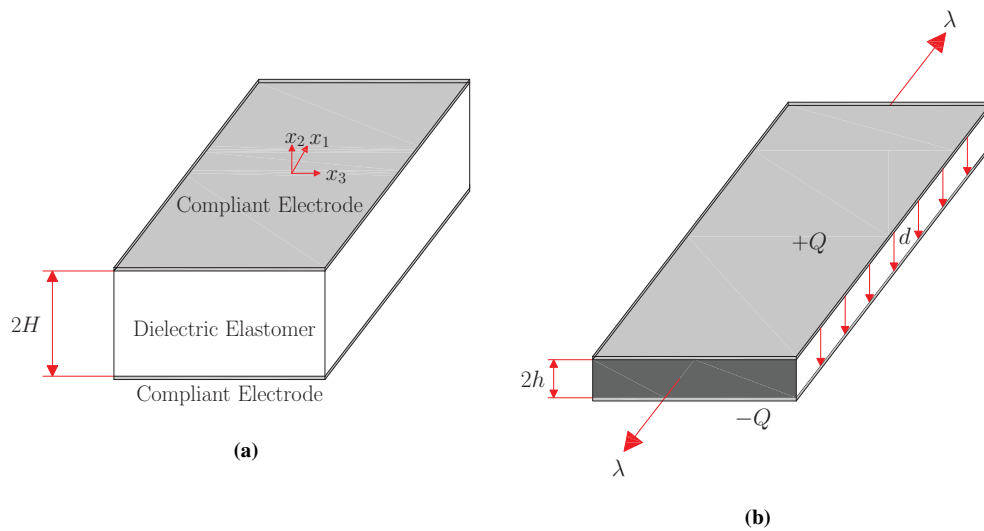


Figure 3.1: Schematics of an infinite DE layer (a) undeformed state, (b) deformed state

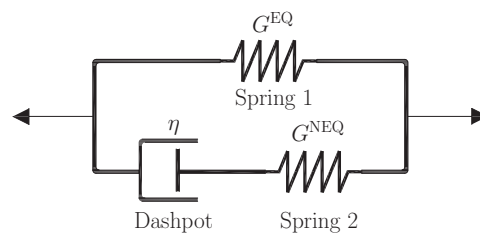


Figure 3.2: Rheological model to illustrate the viscoelastic deformation of a DE layer

3.2.1 Finite-deformation viscoelasticity

As well-established in the literature, DEs exhibit intrinsic viscoelastic properties. Following the theory of finite-deformation viscoelasticity (Hong, 2011), a rheological model is commonly used as shown by Fig. 3.2 to represent two typical types of polymer networks in the DE, i.e., the elastic one (spring 1) and the other relaxing with time and dissipating energy, i.e., the Maxwell element. To describe the viscoelastic deformation, an intermediate (imaginary) state is introduced by fully relaxing the elastomer in the current state as commonly treated in the literature. Here we define the deformation gradient of the current state with respect to the intermediate state as \mathbf{F}^e , and the deformation gradient of the intermediate state as \mathbf{F}^i . The deformation gradient \mathbf{F} of the viscoelastic DE is thus multiplicatively decomposed into an elastic component and an inelastic component, which gives

$$\mathbf{F} = \mathbf{F}^e \mathbf{F}^i. \quad (3.1)$$

where $\mathbf{F}^e = \begin{bmatrix} \lambda^e & 0 & 0 \\ 0 & \lambda_h^e & 0 \\ 0 & 0 & 1 \end{bmatrix}$ and $\mathbf{F}^i = \begin{bmatrix} \lambda^i & 0 & 0 \\ 0 & \lambda_h^i & 0 \\ 0 & 0 & 1 \end{bmatrix}$. Hereinafter, the superscripts "e" and "i" represent the elastic and inelastic components, respectively. Also, as commonly treated in the other studies (Zhao and Suo, 2010; Koh et al., 2011; Shmuel et al., 2012; Zhou et al., 2017), the material incompressibility ensures $\lambda_h = 1/\lambda$, $\lambda_h^e = 1/\lambda^e$, and $\lambda_h^i = 1/\lambda^i$.

Following (Dorfmann and Ogden, 2010), the Piola-Kirchhoff stress S_{ij} and the nominal electric field E_i can be expressed in terms of the Helmholtz energy density function W as

$$S_{ij} = \frac{\partial W}{\partial F_{ij}} - p H_{ji}, \quad (3.2a)$$

$$E_i = \frac{\partial W}{\partial D_i}, \quad (3.2b)$$

where $\mathbf{H} = \mathbf{F}^{-1}$, D_i is the nominal electric displacement component, and p is the Lagrange multiplier introduced for enforcing material incompressibility. Correspondingly, the true stress

σ_{ij} , the true electric displacement d_i , and the true electric field e_i can be determined from those nominal quantities as,

$$\sigma_{ij} = \frac{F_{jk}}{\det(\mathbf{F})} S_{ik}, \quad (3.3a)$$

$$d_i = \frac{F_{ik}}{\det(\mathbf{F})} D_k, \quad (3.3b)$$

$$e_i = H_{ik} E_k. \quad (3.3c)$$

The true electric field \boldsymbol{e} can be given in terms of the gradient of the electrostatic potential V , and experiments suggest $d_i = \varepsilon_0 \varepsilon e_i$ with ε_0 and ε being the permittivity of the vacuum and the relative dielectric constant of the DE medium, respectively.

According to the coupled field theory developed by [Suo et al. \(2008\)](#) and the finite-deformation viscoelasticity model by [Hong \(2011\)](#), the Helmholtz free energy density of a viscoelastic DE can be expressed as

$$W(\mathbf{F}, \mathbf{F}^e, \mathbf{D}) = W^{\text{EQ}}(\mathbf{F}) + W^{\text{NEQ}}(\mathbf{F}^e) + W^P(\mathbf{F}, \mathbf{D}), \quad (3.4)$$

where $W^{\text{EQ}}(\mathbf{F})$ and $W^{\text{NEQ}}(\mathbf{F}^e)$ are the strain energy densities stored in spring 1 and spring 2 as shown in Fig. 3.2, respectively, while the third term is the energy density related to the polarization of the DE. Various hyperelastic constitutive models have been developed to describe the hyperelastic behavior of elastomers. As a case study in this work, the neo-Hookean model is selected for both springs. Accordingly, Eq. (3.4) is reduced to,

$$W = \frac{1}{2} G^{\text{EQ}} (F_{\alpha\beta} F_{\alpha\beta} - 3) + \frac{1}{2} G^{\text{NEQ}} (F_{\alpha\beta} F_{\alpha\theta} H_{\beta\gamma}^i H_{\theta\gamma}^i - 3) + \frac{1}{2\varepsilon_0 \varepsilon} F_{\alpha\beta} F_{\alpha\gamma} D_\beta D_\gamma, \quad (3.5)$$

where G^{EQ} is the shear modulus of the spring 1, and G^{NEQ} is the shear modulus of the Maxwell element, pertinent to the time-dependent and rate-dependent behavior of the DE.

From [\(Reese and Govindjee, 1998\)](#) and [\(Hong, 2011\)](#), the inelastic deformation gradient of the DE is determined by the following inequality which stems from the laws of thermody-

namics, i.e., the free energy of a system never increases,

$$\sigma_{mn}^{\text{NEQ}} Q_{mn}^i \geq 0, \quad (3.6)$$

where

$$\begin{aligned} \sigma_{mn}^{\text{NEQ}} &= \frac{S_{mj}^{\text{NEQ}} F_{nj}^e}{\det \mathbf{F}^e} & \text{with} & \quad S_{mi}^{\text{NEQ}} = \frac{\partial W^{\text{NEQ}}(\mathbf{F}^e)}{\partial F_{mi}^e}, \\ Q_{mn}^i &= \frac{1}{2} (L_{mn}^i + L_{nm}^i) & \text{with} & \quad L_{mn}^i = F_{mj}^e \dot{F}_{jk}^i H_{kp}^i H_{pn}^e, \end{aligned}$$

and the over-dot represents the rate of changes of the quantities due to the rate-dependent behaviors of viscoelastic materials. Mathematically, Eq. (3.6) is automatically satisfied when the thermodynamics evolution law is held, i.e.,

$$Q_{mn}^i = M_{mnjk} \sigma_{jk}^{\text{NEQ}}, \quad (3.7)$$

where $M_{ijkl} = (1/4\eta) (\delta_{ik}\delta_{jl} + \delta_{il}\delta_{jk} - \frac{2}{3}\delta_{ij}\delta_{kl})$, η is the shear viscosity, and δ_{ij} is the Kronecker delta.

In the absence of free body force, free body charge, and free magnetic field, the motion equations, the Faraday's law, and the Gauss's law in the Eulerian form are expressed as,

$$\frac{\partial \sigma_{ji}}{\partial x_j} = \rho \frac{\partial^2 x_i}{\partial t^2}, \quad (3.8a)$$

$$\varepsilon_{kji} \frac{\partial e_i}{\partial x_j} = 0, \quad (3.8b)$$

$$\frac{\partial d_i}{\partial x_i} = 0, \quad (3.8c)$$

where ρ stands for the density of the DE medium. The corresponding boundary conditions are given as

$$(\sigma_{ij} - \sigma_{ij}^*) n_j = t_i, \quad (3.9a)$$

$$\varepsilon_{ijk} (e_j - e_j^*) n_k = 0, \quad (3.9b)$$

$$(d_i - d_i^*) n_i = -\omega, \quad (3.9c)$$

in which "*" represents the fields outside of the material. ω and t_i are the surface charge density and the mechanical traction, respectively. The outer fields are obtained through the following relations

$$\sigma_{ij}^* = \frac{1}{\varepsilon_0} \left(D_i D_j - \frac{1}{2} D_m D_m \delta_{ij} \right), \quad (3.10a)$$

$$d_i^* = \varepsilon_0 e_i^*. \quad (3.10b)$$

3.2.2 Small amplitude fields superimposed on a finitely deformed DE

Here we revisit the problem of Rayleigh-Lamb wave propagation in a DE layer subjected to large deformation investigated by [Shmuel et al. \(2012\)](#) with the consideration of the material viscosity. Upon the current finitely deformed configuration, a small (incremental) time-dependent displacement $u_i = \bar{x}_i(X, t)$ and a small electric displacement $\bar{d}_i(X, t)$ are superimposed, the associated incremental deformation gradient of the DE layer is thus given as,

$$\bar{F}_{ij} = \frac{\partial \bar{x}_i}{\partial X_j} = \frac{\partial u_i}{\partial X_j} \quad (3.11)$$

Herein and throughout the paper a quantity with over-bar represents an incremental quantity. The corresponding motion equations and the Maxwell equations can be rewritten in terms of the incremental quantities as,

$$\frac{\partial \bar{\sigma}_{ji}}{\partial x_j} = \rho \frac{\partial^2 u_i}{\partial t^2}, \quad (3.12a)$$

$$\varepsilon_{kji} \frac{\partial \bar{e}_i}{\partial x_j} = 0, \quad (3.12b)$$

$$\frac{\partial \bar{d}_i}{\partial x_i} = 0. \quad (3.12c)$$

Considering the constitutive equations (3.2) and the relations between the true and nominal electroelastic fields in Eq. (3.3), Eqs. (3-12a) and (3-12b) are expressed in terms of the

Helmholtz free energy density function in general sense, i.e.,

$$\frac{\partial}{\partial x_j} \left(\frac{\partial^2 W}{\partial F_{ik} \partial F_{mn}} F_{jk} F_{n\alpha} R_{m\alpha} + \frac{\partial^2 W}{\partial F_{ik} \partial F_{mn}^i} F_{jk} \bar{F}_{mn}^i + \frac{\partial^2 W}{\partial F_{ik} \partial D_m} F_{jk} H_{m\alpha} \bar{D}_\alpha + p R_{ji} - \bar{p} \delta_{ji} \right) = \rho u_{i,tt}, \quad (3.13a)$$

$$\varepsilon_{kji} \frac{\partial}{\partial x_j} \left(H_{ik} \frac{\partial^2 W}{\partial F_{pq} \partial D_k} F_{Aq} R_{pA} + H_{ik} \frac{\partial^2 W}{\partial D_m \partial D_k} H_{mA} \bar{D}_A \right) = 0, \quad (3.13b)$$

in which $R_{ij} = \bar{F}_{ik} H_{kj}$ and $\bar{F}_{mn}^i = F_{cn} R_{m\alpha}^i$. Specially for the viscoelastic DE with Neo-Hookean model, these equations are further reduced to,

$$\frac{\partial}{\partial x_j} \left[\frac{d_j \bar{d}_i + d_i \bar{d}_j}{\varepsilon \varepsilon_0} - G^{\text{NEQ}} F_{An} R_{mA}^i \left(F_{i\alpha} F_{jk} H_{\alpha m}^i H_{k\beta}^i H_{n\beta}^i + F_{i\alpha} F_{jk} H_{\alpha\beta}^i H_{km}^i H_{n\beta}^i \right) - \bar{p} \delta_{ji} \right] + \quad (3.14a)$$

$$\frac{\partial}{\partial x_j} \left[\left(\frac{d_A d_j R_{iA}}{\varepsilon \varepsilon_0} + G^{\text{EQ}} F_{Ak} F_{jk} R_{iA} + F_{An} F_{jk} G^{\text{NEQ}} R_{iA} H_{k\alpha}^i H_{n\alpha}^i \right) + p R_{ji} \right] = \rho u_{i,tt},$$

$$\varepsilon_{kji} \frac{\partial}{\partial x_j} \left[F_{Bk} H_{ik} (\bar{d}_B + d_p R_{pB} + d_A R_{BA}) \right] = 0. \quad (3.14b)$$

So far the general equations of motion for a neo-Hookean viscoelastic DE layer with the consideration of small fields superimposed on finite deformations are obtained. For a case study, we will focus on the plane-strain problem with $d_1 = d_3 = 0$, $d_2 \neq 0$, $\lambda_1 = \lambda$, $\lambda_2 = \lambda_h$, $\lambda_3 = 1$, $u_1 = u_1(x_1, x_2, t)$, $u_2 = u_2(x_1, x_2, t)$, $u_3 = 0$, $\bar{d}_1 = \bar{d}_1(x_1, x_2, t)$, $\bar{d}_2 = \bar{d}_2(x_1, x_2, t)$, and $\bar{p} = \bar{p}(x_1, x_2, t)$. Correspondingly, the incremental non-equilibrium true stresses $\bar{\sigma}^{\text{NEQ}}$ are obtained as,

$$\bar{\sigma}_{11}^{\text{NEQ}} = G^{\text{NEQ}} \left(\frac{\lambda}{\lambda^i} \right)^2 \left(R_{11} - \frac{\lambda R_{11}^i}{\lambda^i} \right), \quad (3.15a)$$

$$\bar{\sigma}_{12}^{\text{NEQ}} = G^{\text{NEQ}} \left[R_{12} \left(\frac{\lambda^i}{\lambda} \right)^2 - \frac{\lambda^i R_{12}^i}{\lambda} \right], \quad (3.15b)$$

$$\bar{\sigma}_{21}^{\text{NEQ}} = G^{\text{NEQ}} \left[R_{21} \left(\frac{\lambda}{\lambda^i} \right)^2 - \frac{\lambda R_{21}^i}{\lambda^i} \right], \quad (3.15c)$$

$$\bar{\sigma}_{22}^{\text{NEQ}} = G^{\text{NEQ}} \left(\frac{\lambda^i}{\lambda} \right)^2 \left(R_{22} - \frac{\lambda^i R_{22}^i}{\lambda} \right), \quad (3.15d)$$

Substituting Eq. (3.15) into the thermodynamics evolution law, i.e., Eq. (3.7), the inelastic stretch ratios are obtained as,

$$\frac{d\lambda^i}{dt} = \frac{G^{\text{NEQ}}}{6\eta\lambda^3\lambda^i R_{11}^i} \left[R_{22} (\lambda^i)^5 - 2\lambda^4 (R_{11}\lambda^i - \lambda R_{11}^i) - \frac{(\lambda^i)^6 R_{22}^i}{\lambda} \right], \quad (3.16a)$$

$$\frac{d\lambda_h^i}{dt} = \frac{G^{\text{NEQ}}}{6\eta\lambda (\lambda^i)^5 R_{22}^i} \left[\frac{2(\lambda^i)^6 R_{22}^i}{\lambda} - 2R_{22} (\lambda^i)^5 + \lambda^4 (R_{11}\lambda^i - \lambda R_{11}^i) \right]. \quad (3.16b)$$

Particularly when $d\lambda^i/dt = d\lambda_h^i/dt = 0$ and $\lambda^i = \lambda$, the response of the DE layer recovers that of the purely elastic DE layer. When considering the material viscosity, we define time-dependent functions $K(t)$ and $G(t)$ to relate λ^i to λ and R_{mn}^i to R_{mn} , respectively. For the limiting case when $K(t) = G(t) = 1$, the medium is fully relaxed and the response of the DE layer recovers that for a non-viscous DE layer. Therefore, λ^i and R_{mn}^i can be calculated as

$$\lambda^i = \lambda K(t), \quad (3.17a)$$

$$R_{11}^i = R_{11} G(t), \quad (3.17b)$$

$$R_{22}^i = R_{22} G(t), \quad (3.17c)$$

$$R_{12}^i = \frac{\lambda^2 (R_{12} + R_{21}) G(t)}{\lambda^2 + 1}, \quad (3.17d)$$

$$R_{21}^i = \frac{(R_{12} + R_{21}) G(t)}{\lambda^2 + 1}. \quad (3.17e)$$

By substituting Eq. (3.17) into Eq. (3.16), it is obtained that

$$\dot{K}(t) = \frac{G^{\text{NEQ}}}{6\eta G(t) K(t)} \left\{ G(t) K(t)^6 - 2 [K(t) - G(t)] - K(t)^5 \right\}, \quad (3.18a)$$

$$G(t) = \frac{K(t)^7 + 2K(t)^5 + 2K(t)^3 + K(t)}{K(t)^8 + 2K(t)^6 + 2K(t)^2 + 1}. \quad (3.18b)$$

Consequently, by substituting Eq. (3.17) into equations of motion (3-14a) and (3-14b), we have

$$\begin{aligned}
R_{11,12} \left(\lambda^2 G^{\text{EQ}} + \frac{G^{\text{NEQ}}}{K(t)^2} + p \right) + \left(\frac{G^{\text{EQ}}}{\lambda^2} + K(t)^2 G^{\text{NEQ}} + \frac{d_2^2}{\varepsilon \varepsilon_0} \right) R_{12,22} + \\
p R_{21,22} + \frac{d_2 \bar{d}_{1,22}}{\varepsilon \varepsilon_0} - G(t) G^{\text{NEQ}} \left\{ \frac{2}{K(t)^3} R_{11,12} + \frac{1}{1 + \lambda^2} \right.
\end{aligned} \tag{3.19a}$$

$$\left. \left[\frac{1}{K(t)} + \lambda^2 K(t) \right] (R_{12,22} + R_{21,22}) \right\} + \bar{p}_{,12} = \rho \ddot{u}_{1,2},$$

$$\begin{aligned}
R_{22,12} \left(\frac{G^{\text{EQ}}}{\lambda^2} + G^{\text{NEQ}} K(t)^2 + \frac{d_2^2}{\varepsilon \varepsilon_0} + p \right) + \left(G^{\text{EQ}} \lambda^2 + \frac{G^{\text{NEQ}}}{K(t)^2} \right) R_{21,11} + \\
p R_{12,11} - G(t) G^{\text{NEQ}} \left\{ 2K(t)^3 R_{22,12} + \frac{1}{1 + \lambda^2} \left[K(t) + \frac{\lambda^2}{K(t)} \right] \right.
\end{aligned} \tag{3.19b}$$

$$\left. (R_{21,11} + R_{12,11}) \right\} + \frac{d_2}{\varepsilon \varepsilon_0} (2\bar{d}_{2,12} + \bar{d}_{1,11}) + \bar{p}_{,12} = \rho \ddot{u}_{2,1},$$

$$\bar{d}_{2,1} + 2d_2 R_{22,1} = 0, \tag{3.19c}$$

$$\bar{d}_{1,2} + d_2 (R_{12,2} + R_{21,2}) = 0. \tag{3.19d}$$

3.2.3 Wave propagation in a DE layer

In this section, we focus on the electroelastic wave due to the harmonic excitation along x_1 direction superimposed on the deformed DE configuration induced by both the pre-stretch and the electric displacement. Stream functions $\phi(x_1, x_2, t)$ and $\psi(x_1, x_2, t)$ are introduced so that the material incompressibility $u_{1,1} + u_{2,2} = 0$ and the Gauss's equation (3-12c) are satisfied automatically, i.e.,

$$u_1 = \phi_{,2}(x_1, x_2, t), \quad u_2 = -\phi_{,1}(x_1, x_2, t), \tag{3.20}$$

$$\bar{d}_1 = \psi_{,2}(x_1, x_2, t), \quad \bar{d}_2 = -\psi_{,1}(x_1, x_2, t).$$

The solution of the wave propagation takes the time-dependency in the form of $e^{-i\omega t}$ and a periodicity along the x_1 -axis in the form of e^{ikx_1} , as

$$\phi = A e^{ik(ct-x_1)} e^{qkx_2}, \tag{3.21a}$$

$$\psi = B k e^{ik(ct-x_1)} e^{qkx_2}, \tag{3.21b}$$

where A and B are constants to be determined, q is the attenuation factor, ω is the angular frequency and k is the associated wavenumber such that the wave velocity is determined as $c = \omega/k$. By substituting Eq. (3.20) into Eq. (3.19) and rearranging the obtained governing equations, we have

$$\begin{aligned} & \left[\lambda^2 G^{\text{EQ}} + G^{\text{NEQ}} \left(\frac{G(t)}{K(t)} + \frac{1}{K(t)^2} \right) \right] \phi_{,1111} + \phi_{,2222} \\ & \left[\frac{G^{\text{EQ}}}{\lambda^2} + G^{\text{NEQ}} \left(G(t)K(t) + K(t)^2 \right) + \frac{d_2^2}{\varepsilon_r \varepsilon_0} \right] + \\ & \left[\left(\lambda^2 + \frac{1}{\lambda^2} \right) G^{\text{EQ}} + \frac{d_2^2}{\varepsilon \varepsilon_0} \right] \phi_{,1122} + \\ & G^{\text{NEQ}} \left[G(t)K(t) - 2 \left(G(t)K(t)^3 + \frac{G(t)}{K(t)^3} \right) + \right. \\ & \left. \frac{G(t)}{K(t)} + K(t)^2 + \frac{1}{K(t)^2} \right] \phi_{,1122} + \frac{d_2 (\psi_{,11} + \psi_{,22})_{,2}}{\varepsilon \varepsilon_0} = \\ & \rho (\ddot{\phi}_{,11} + \ddot{\phi}_{,22}) \end{aligned} \quad (3.22a)$$

$$d_2 (\phi_{,112} - \phi_{,222}) - 2d_2 \phi_{,112} = \psi_{,11} + \psi_{,22} \quad (3.22b)$$

Substituting Eq. (3.21) into the governing equations (3.22), a system of two linear homogeneous equations with unknown coefficients A and B is obtained. In order to have non-trivial solutions, the determinant of the coefficient matrix must equal to zero, which results in a bi-cubic polynomial equation to determine q as

$$(q^2 - 1)(a_1 q^4 + a_2 q^2 + a_3) = 0, \quad (3.23)$$

where the coefficients a_1 , a_2 , and a_3 are defined as

$$a_1 = \frac{G^{\text{EQ}}}{\lambda^2} + G^{\text{NEQ}} \left[K(t)^2 - \frac{G(t) \left(\lambda^2 K(t) + \frac{1}{K(t)} \right)}{\lambda^2 + 1} \right], \quad (3.24a)$$

$$\begin{aligned} a_2 = & -G^{\text{NEQ}} \left\{ 2G(t) \left[\frac{\lambda^2 K(t) + \frac{1}{K(t)}}{\lambda^2 + 1} - \left(K(t)^3 + \frac{1}{K(t)^3} \right) \right] + \right. \\ & \left. K(t)^2 + \frac{1}{K(t)^2} \right\} + \rho c^2 - \left(\lambda^2 + \frac{1}{\lambda^2} \right) G^{\text{EQ}}, \end{aligned} \quad (3.24b)$$

$$a_3 = \lambda^2 G^{\text{EQ}} + G^{\text{NEQ}} \left[\frac{1}{K(t)^2} - \frac{G(t) \left(\lambda^2 K(t) + \frac{1}{K(t)} \right)}{\lambda^2 + 1} \right] - \rho c^2. \quad (3.24c)$$

From Eq. (3.23), it can be seen that there are six possible roots for q , namely, $q_1 = -1$, $q_2 = 1$, $q_3 = -q_4$, and $q_5 = -q_6$. It is important to mention that for q_1 and q_2 , the unknown coefficients $A_n = 0$ while the coefficients B_n are still not determined. However, for q_3, q_4, q_5 , and q_6 , there exists dependency between the coefficients A_n and B_n such that $B_n = -q_n d_2 A_n$ ($n = 3, 4, 5, 6$). Therefore, the general solution for the stream functions $\phi(x_1, x_2, t)$ and $\psi(x_1, x_2, t)$ can be written as a linear combination of all the roots in the following format,

$$\phi = e^{ik(ct-x_1)} \sum_{n=3}^6 A_n e^{kx_2 q_n}, \quad (3.25a)$$

$$\psi = k e^{ik(ct-x_1)} \sum_{n=1}^6 B_n e^{kx_2 q_n}. \quad (3.25b)$$

Moreover, to satisfy a decaying condition at $x_2 \rightarrow \pm\infty$ and the Laplace equation outside the DE layer, the following stream functions are considered for the exterior fields,

$$\mu^* = iC_1 k e^{-kx_2} e^{ik(ct-x_1)} \quad (x_2 \geq h), \quad (3.26a)$$

$$\nu^* = iC_2 k e^{kx_2} e^{ik(ct-x_1)} \quad (x_2 \leq -h), \quad (3.26b)$$

where the exterior electric field components are given by

$$\bar{e}_1^* = \begin{cases} -\mu_{,1}^* & x_2 \geq h \\ -\nu_{,1}^* & x_2 \leq -h \end{cases}, \quad (3.27a)$$

$$\bar{e}_2^* = \begin{cases} -\mu_{,2}^* & x_2 \geq h \\ -\nu_{,2}^* & x_2 \leq -h \end{cases}. \quad (3.27b)$$

In summary, there exists a set of eight constants to be determined, namely $A_3, A_4, A_5, A_6, B_1, B_2, C_1$, and C_2 , from the appropriate boundary conditions across the upper and the lower surfaces of the DE layer at $x_2 = \pm h$, i.e.,

$$\bar{\sigma}_{22} = 0, \quad \bar{\sigma}_{12} = 0, \quad \bar{d}_2^* - \bar{d}_2 = 0, \quad \bar{e}_1^* - \bar{e}_1 = 0. \quad (3.28)$$

where

$$\bar{\sigma}_{22} = -\bar{p} + \sum_{n=1}^6 \left\{ \left[\frac{G^{\text{EQ}}}{\lambda^2} + \frac{d_2^2}{\varepsilon\varepsilon_0} + p + G^{\text{NEQ}}K(t)^2 (1 - 2G(t)K(t)) \right] ik^2 A_n q_n e^{kx_2 q_n} + \frac{2id_2 k^2 B_n e^{kx_2 q_n}}{\varepsilon\varepsilon_0} \right\}, \quad (3.29a)$$

$$\bar{\sigma}_{12} = \sum_{n=1}^6 k^2 A_n q_n^2 e^{kx_2 q_n} \left(\frac{d_2^2}{\varepsilon\varepsilon_0} + \frac{G^{\text{EQ}}}{\lambda^2} + G^{\text{NEQ}}K(t)^2 \right) - k^2 A_n e^{kx_2 q_n} \left[-p + \frac{G^{\text{NEQ}}G(t)}{\lambda^2 + 1} \left(\frac{\lambda^2 K(t)^2 + 1}{K(t)} \right) (q_n^2 + 1) \right] +, \quad (3.29b)$$

$$\frac{e^{kx_2 q_n} (d_2 k^2 B_n q_n)}{\varepsilon\varepsilon_0}$$

$$\bar{e}_1 = \sum_{n=1}^6 \left[d_2 A_n (q_n^2 + 1) + B_n q_n \right] k^2 e^{kx_2 q_n}, \quad (3.29c)$$

$$\bar{d}_2 = \sum_{n=1}^6 ik^2 B_n e^{kx_2 q_n}. \quad (3.29d)$$

It is noted that the solution for the incremental pressure is given from

$$\bar{p} = (P_1 e^{-kx_2} + P_2 e^{kx_2}) k e^{ik(ct-x_1)}, \quad (3.30)$$

where P_1 and P_2 are calculated via Eqs. (3-19a) and (3-19b).

The boundary conditions in Eq. (3.28) constitute a system of eight linear homogeneous equations to determine the eight unknown coefficients. Non-trivial solutions exist only when the determinant of the coefficient matrix vanishes, leading to an equation which can be regarded as the extension of Rayleigh-Lamb transcendental equation for a viscoelastic DE layer with finite deformation. Utilizing the transcendental equation, the dispersion relation, i.e., the relation between the wavenumber k or wavelength and the velocity c , is thus obtained. It is worth mentioning that for a given wavenumber, there may exist various wave frequencies satisfying the dispersion relation, which corresponds to different modes of wave propagation. Here a numerical iterative root-finding method is applied to calculate the admissible c values for a range of wavenumber k . Then the dependence of the dispersion relation of the wave propagation in a viscoelastic DE layer on the electric field, the pre-stretch, the material viscosity, and the relaxation status of the medium will be discussed in detail in the next section.

3.3 Numerical Results and Discussion

In this section, numerical simulation results will be demonstrated to show the factors that influence the wave dispersion in a viscoelastic DE layer, including the applied electromechanical loads, the material viscoelasticity and the relaxation status of the material. Phase velocity denoted by c is the rate at which the phase of the wave propagates through the layer. On the other hand, the envelope shape of the wave propagates with another velocity called group velocity (denoted by V_G), which expresses the rate at which energies are transported. Here, to present the results in a more convenient way, we introduce the dimensionless quantities $\hat{d} = d_2/\sqrt{G^{\text{EQ}}\varepsilon\varepsilon_0}$, $\hat{t} = G^{\text{NEQ}}t/\eta$, $\hat{k} = kh$, $\hat{c} = c/c_B$, and $\hat{V}_G = V/c_B$ with $c_B = \sqrt{G^{\text{EQ}}/\rho}$ representing the bulk shear wave velocity in a purely elastic medium and $\hat{\omega} = \hat{c}\hat{k}$. Also, a material parameter $\chi = G^{\text{EQ}}/(G^{\text{EQ}} + G^{\text{NEQ}})$ indicating the fraction of the polymer networks that have time-independent behavior is introduced to represent the viscoelasticity of the material. The material becomes purely elastic when $\chi = 1$, while it is a viscous fluid when $\chi = 0$.

From Eqs. (3-29a) and (3-29b) it is found that the incremental stresses at boundaries ($x_2 = \pm h$) of the viscoelastic DE layer depend on the time-dependent functions $K(t)$ and $G(t)$, which means that the dispersion relation is contingent on the relaxation status of the viscoelastic DE medium. Therefore, to obtain the dispersion relation, the relaxation status of the DE medium at the beginning of the wave propagation, i.e., $K(0)$ and $G(0)$, must be prescribed first through Eq. (3.18). From Eq. (3-17a), it is noted that the value of $K(0)$ ranges from $1/\lambda$ to 1. Figs. 3.3a and 3.3b depict the variation of $K(\hat{t})$ and $G(\hat{t})$ with the normalized time \hat{t} for different relaxation status of the DE medium at the beginning of wave propagation ($K(0)$). It is found that for all the cases, both of $K(\hat{t})$ and $G(\hat{t})$ increase with time. As the DE medium continues to relax with time, both of $K(\hat{t})$ and $G(\hat{t})$ converge to 1, corresponding to the fully relaxed state of the DE layer.

As mentioned previously, for any given value of excitation frequency $\hat{\omega}$, there exist dif-

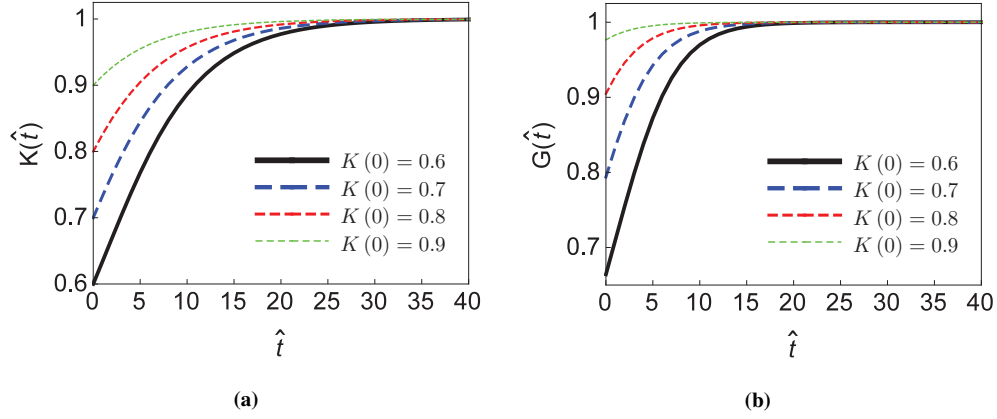


Figure 3.3: variation of (a) $K(\hat{t})$ and (b) $G(\hat{t})$ with normalized time \hat{t}

ferent values of wavenumber \hat{k}_m which satisfy the dispersion relation and correspondingly represent different modes of the wave propagation with phase velocity of $\hat{c}_m = \hat{\omega}/\hat{k}_m$. It has been shown that for both purely elastic medium (Rayleigh, 1885; Lamb, 1917) and hyperelastic dielectric medium (Shmuel et al., 2012), the wave propagation can be decomposed into two modes with respect to the mid-plane of the layer, i.e., symmetric (extensional) and antisymmetric (flexural) modes. For the symmetric mode, the displacement u_2 in the x_2 -axis direction and the incremental normal stress $\bar{\sigma}_{22}$ distribute symmetrically while the incremental shear stress $\bar{\sigma}_{21}$ and the incremental electric displacement \bar{d}_2 distribute asymmetrically with respect to the mid-plane. As for the antisymmetric mode, the distribution of these quantities is in the opposite way. For the current case with the wave propagation in a viscoelastic DE, the same decomposition of wave modes still holds true. Hereinafter, we will focus on presenting the results on the fundamental symmetric and antisymmetric modes, i.e., the lowest two modes. It should be mentioned that these two modes have finite value of velocity for the limiting case of long wave propagation when $\hat{k}_m \rightarrow 0$. However, for other higher modes, the phase velocity \hat{c}_m approaches to infinite when $\hat{k}_m \rightarrow 0$. As the first step, the solution technique presented in this work is validated by comparing with the results from the literature for a purely hyperelastic case with $\chi = 1$ (Shmuel et al., 2012). For such a special case, the dispersion relation is independent of $K(t)$ since there is no material relaxation for a purely elastic medium. The variation

of the normalized phase velocity with the normalized wavenumber is plotted in Fig. 3.4 for an unstretched DE ($\lambda = 1$) under different electrical loads ($\hat{d} = 0$ and $\hat{d} = 1$ for example). Excellent agreement is observed for both the symmetric and antisymmetric modes. For the limiting case of short waves ($\hat{k} \rightarrow \infty$), the two modes coincide and reach the velocity of the surface wave. Particularly, the wave speed $\hat{c} = 0.955$ for the Rayleigh surface wave without applying electrical load ($\hat{d} = 0$). On the other hand, for the limiting case of long waves, the fundamental symmetric mode reaches the well-known result of $\hat{c} = 2$ for the purely elastic wave ($\hat{d} = 0$).

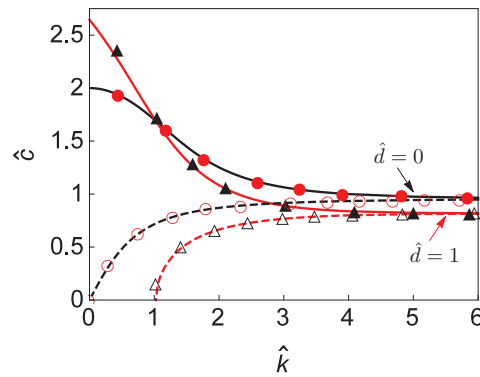


Figure 3.4: Variation of normalized phase velocity with normalized wavenumber for an unstretched DE under different electrical loads. The continuous and dashed curves correspond to the symmetric mode and the antisymmetric mode, respectively. The scattered markers correspond to the results obtained by Shmuel et al. (2012) with filled and empty markers representing symmetric and antisymmetric modes, respectively.

To investigate the characteristics of the wave propagation in the DE medium with the consideration of both material viscoelasticity and electromechanical coupling, we focus on the dispersion relations. Under different electromechanical loading conditions, Figs. 3.5 and 3.6 plot the variation of the normalized phase velocity and the normalized group velocity with the normalized wavenumber at different relaxation state of the viscoelastic DE medium, for example, $K(\hat{t})$ varies from a partially relaxed state of 0.8 to a fully relaxed state of 1.0. It is observed that for large values of \hat{k} , in other words, in the range of short waves, the velocity of the symmetric and the antisymmetric modes converges to the same value which is corresponding to the speed of the surface wave propagating through a DE half space as expected. It is also noted

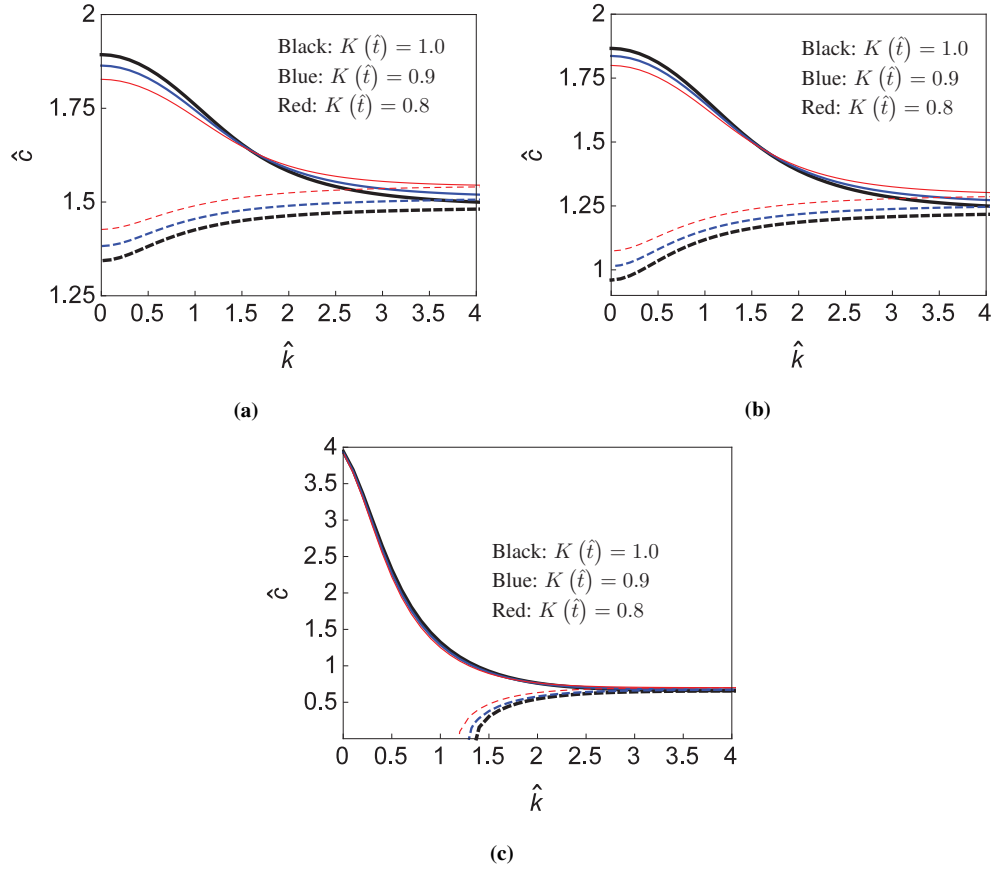


Figure 3.5: Variation of normalized phase velocity with respect to normalized wavenumber for different values of $K(\hat{t})$ when (a) $\hat{d} = 0$, $\lambda = 1.5$ and $\chi = 0.8$, (b) $\hat{d} = 0$, $\lambda = 1.25$ and $\chi = 0.8$, and (c) $\hat{d} = 2$, $\lambda = 1.5$ and $\chi = 0.8$. The continuous and dashed curves correspond to the symmetric mode and the antisymmetric mode, respectively.

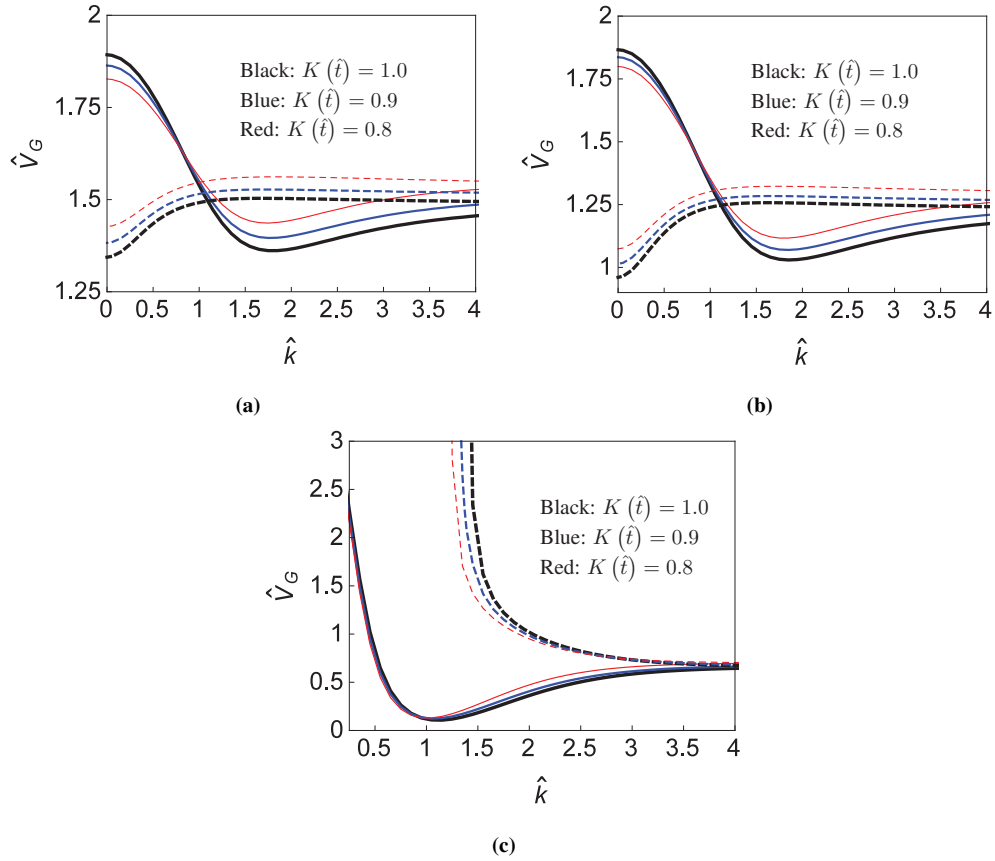


Figure 3.6: Variation of normalized group velocity with respect to normalized wavenumber for different values of $K(\hat{t})$ when (a) $\hat{d} = 0$, $\lambda = 1.5$ and $\chi = 0.8$, (b) $\hat{d} = 0$, $\lambda = 1.25$ and $\chi = 0.8$, and (c) $\hat{d} = 2$, $\lambda = 1.5$ and $\chi = 0.8$. The continuous and dashed curves correspond to the symmetric mode and the antisymmetric mode, respectively.

(a)						(b)					
λ	\hat{d}	\hat{k}_P^{int}	\hat{k}_G^{int}	\hat{c}^{int}	\hat{V}_G^{int}	\hat{d}	λ	\hat{k}_P^{int}	\hat{k}_G^{int}	\hat{c}^{int}	\hat{V}_G^{int}
	0.0	1.58	0.75	1.64	1.67		1.25	1.58	0.75	1.48	1.53
	0.5	1.61	0.79	1.61	1.56		1.50	1.58	0.75	1.64	1.67
1.5	1.0	1.71	0.84	1.49	1.24	0	1.75	1.58	0.75	1.84	1.85
	1.5	1.8	0.89	1.26	0.79		2.00	1.58	0.75	2.06	2.07
	2.0	1.93	0.97	0.78	0.12		2.25	1.58	0.75	2.29	2.3
	0.0	1.58	0.75	2.06	2.07		1.25	1.71	0.84	1.30	1.07
	0.5	1.61	0.79	2.03	1.99		1.50	1.71	0.84	1.49	1.24
2	1.0	1.71	0.84	1.94	1.74	1	1.75	1.71	0.84	1.71	1.48
	1.5	1.8	0.89	1.76	1.42		2.00	1.71	0.84	1.94	1.74
	2.0	1.93	0.97	1.43	1.03		2.25	1.71	0.84	2.19	2.01

Table 3.1: Effect of (a) electric displacement \hat{d} and (b) pre-stretch λ on the particular wavenumber at which wave propagates independent of the relaxation status of the medium.

that for a less relaxed DE medium with lower value of $K(\hat{t})$, the convergence becomes faster, which means that the relaxation status of the viscoelastic medium affects the surface wave propagation. Another important point is that for the fundamental symmetric mode, the phase velocity monotonically decreases with the wave number. While the curve of the group velocity is non-monotonic as observed from Fig. 3.6. Moreover, for the symmetric mode waves, it is seen that in the range of long waves, both phase and group velocities increase with the more relaxation of the DE medium. However, a reversed trend is found in the range of short waves propagating through the DE layer. It is interesting to note from Fig. 3.5 that for the symmetric mode wave propagation, regardless of the values of $K(\hat{t})$, all the dispersion curves have an intersection point (\hat{k}_P^{int}) under the same electromechanical loading condition. It means that the material viscosity has no effect on such wave propagation with a particular wavenumber. Similar phenomenon is observed for the group velocity as well in Fig. 3.6. However, the intersection point \hat{k}_G^{int} for the group velocity is different from that of the phase velocity. The variation of this particular wavenumber with the applied mechanical and electrical loads is summarized in Table 3.1. It is found that only the applied electrical load can alter this wavenumber. This finding will offer avenue for controlling wave propagation in a viscous dielectric medium. For example, if a wave with a certain wavenumber is considered for a specific application, one can adjust the electrical load on the dielectric medium to make the wave speed independent of the relaxation status of the medium or the material viscoelasticity. It thus provides an insight in eliminating the material viscoelasticity effect on the wave propagation in a DE medium by applying electrical loads.

With regard to the antisymmetric mode, the phase velocity of the waves decreases when propagating in a more relaxed DE medium. It is interesting to note from Fig. 3.5c that when the applied electric displacement increases to a certain value, for example $\hat{d} = 2$, the phase velocity decays for the long waves until it reaches a vanishing value. The wavenumber corresponding to the vanishing phase velocity can be perceived as a threshold of the wavenumber. For long waves with wavenumber less than this threshold, the antisymmetric mode wave does not exhibit

in the medium. This is due to the surface instability of the DE layer under the condition that the pre-stretch ratio is fixed, which is also observed for the wave propagation in a purely elastic medium (Shmuel et al., 2012). The reason behind this is that the applied electric displacement induces tension reduction since the DE layer is clamped at its two ends without free elongation. It is also found from Fig. 3.5c that for a more relaxed medium, the antisymmetric mode wave spectrum becomes narrower due to the loss of the surface stability. As for the group velocity, it is observed from Figs. 3.6a and 3.6b that it decreases with the more relaxation of the medium. However, such a trend in the group velocity is reversed once the loss of the surface stability of the medium occurs.

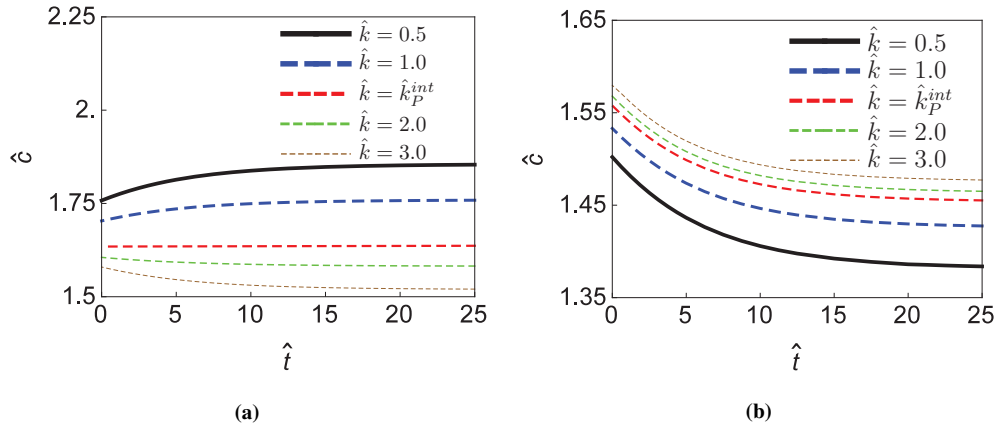


Figure 3.7: Variation of normalized phase velocity of (a) symmetric and (b) antisymmetric modes with normalized time when $\hat{d} = 0$, $\lambda = 1.5$, $\chi = 0.8$, and $K(0) = 0.7$.

Since the DE layer is viscoelastic, the wave velocity varies with time due to the material relaxation. Figs. 3.7a and 3.7b clearly show the variation of the normalized phase velocity \hat{c} with the normalized time \hat{t} for both symmetric and antisymmetric modes. In this case study, the applied electromechanical loads are fixed as $\hat{d} = 0$, $\lambda = 1.5$, the material viscoelasticity is selected as $\chi = 0.8$, and the wavenumber \hat{k} varies. As time passes, the phase velocity reaches a constant value, which is corresponding to a steady state when the material is fully relaxed. It is observed from Fig. 3.7a that for the symmetric mode, when the wavenumber is less than a particular number, i.e., $\hat{k} < \hat{k}_P^{\text{int}}$, the phase velocity rises with the wavenumber. However, when

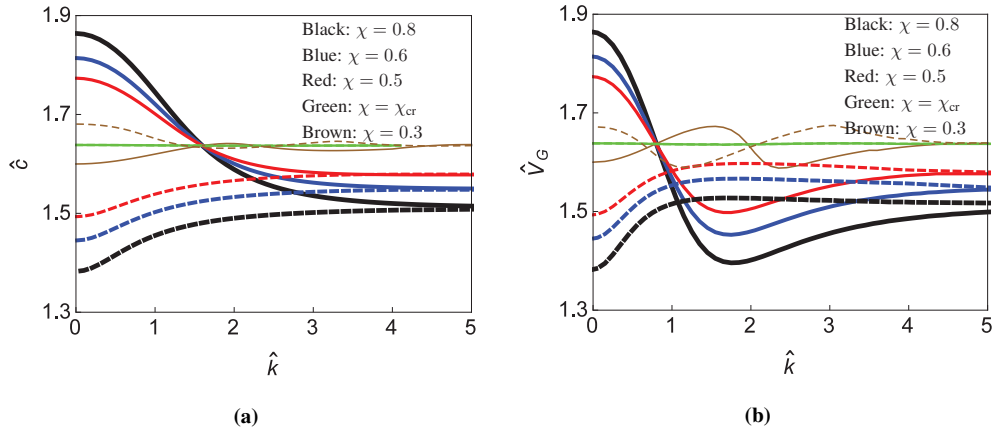


Figure 3.8: Variation of (a) normalized phase velocity \hat{c} and (b) normalized group velocity \hat{V}_G with normalized wavenumber \hat{k} for different material viscosity χ ($\lambda = 1.5$, $\hat{d} = 0$, and $K(\hat{t}) = 0.9$). The continuous and dashed curves correspond to the symmetric mode and the antisymmetric mode, respectively.

(a)				(b)			
λ	\hat{d}	$K(\hat{t})$	χ_{cr}	λ	$K(\hat{t})$	\hat{d}	χ_{cr}
		0.70	0.504			0.0	0.638
1.5	0.5	0.75	0.441	1.5	0.7	0.5	0.504
		0.08	0.373			1.0	0.359
		0.85	0.302			1.5	0.357
		0.90	0.231			2.0	0.356

$K(\hat{t})$	\hat{d}	λ	χ_{cr}
		1.25	0.308
0.9	0.0	1.50	0.328
		1.75	0.395
		2.00	0.462
		2.25	0.526

Table 3.2: Effect of (a) material relaxation status $K(\hat{t})$, (b) normalized electric displacement \hat{d} , and (c) pre-stretch λ , on the critical value of material viscosity χ_{cr} .

$\hat{k} > \hat{k}_p^{\text{int}}$, the phase velocity descends with the wavenumber. Particularly when the wavenumber $\hat{k} = \hat{k}_p^{\text{int}}$, the wave always propagates at a steady state with a constant phase velocity and the material relaxation has no effect on the symmetric mode wave. As for the antisymmetric mode demonstrated by Fig. 3.7b, all the velocity curves descend and reach a steady state when the DE medium is fully relaxed. It is also found that the antisymmetric mode wave with larger wave number, i.e., shorter wave, propagates faster.

In order to see the material viscosity effect on the wave propagation, Figs. 3.8a and 3.8b illustrate the dispersion relation, i.e., the variation of the normalized phase and group velocities versus the normalized wavenumber at a particular relaxation state ($K(\hat{t}) = 0.9$) for different values of the material viscoelasticity χ when the electromechanical loads are fixed as $\lambda = 1.5$ and $\hat{d} = 0$. For the antisymmetric mode wave propagation, both the phase and group velocities increase with the decreasing of χ . It means that the antisymmetric mode wave propagates faster in a more viscous medium. However, for the symmetric mode wave, there is a transition point for the wavenumber, i.e., the intersection points as observed in Figs. 3.5 and 3.6. The effect of the material viscosity on the wave propagation varies depending on the wavenumber. It is observed that the long waves propagate faster while the short waves propagate slower in the more elastic medium (larger χ). For example, both the phase velocity and the group velocity decrease with an increasing χ for the wave with the wavenumber greater than the transition wave number, i.e., $\hat{k} > \hat{k}_p^{\text{int}}$ and $\hat{k} > \hat{k}_G^{\text{int}}$, respectively. A reverse trend is observed for the wave with the wavenumber less than this transition value. The existence of the transition point for the wavenumber means that even for a viscoelastic medium, the wave with a particular wavenumber is able to propagate through the medium without being influenced by the material viscosity. It should be mentioned that the above mentioned conclusions on the viscosity effect are only applicable when the material viscoelasticity indicator χ is greater than a certain value. It is interesting to find when the DE is getting more viscous, i.e., when χ decreases to reach a critical value χ_{cr} , both the symmetric mode and antisymmetric mode waves become non-dispersive. Meanwhile, the velocity of the two modes reaches the same value. For the DE

with material viscosity $\chi < \chi_{cr}$, relatively long waves ($\hat{k} < \hat{k}_p^{int}$) propagate slower in the more viscous medium. However, the material viscosity effect on the wave propagation of relatively short waves ($\hat{k} > \hat{k}_p^{int}$) becomes more complicated, while becomes negligible for the surface waves as both the phase and group velocities converge to the same values for the case when $\chi = \chi_{cr}$. It is thus concluded that the material viscosity has significant effect upon the wave propagation in the medium. For certain viscoelastic medium, i.e., when the material viscosity $\chi = \chi_{cr}$, the wave propagation even becomes non-dispersive. It is also found that this critical material viscosity χ_{cr} depends on the relaxation status, the mechanical pre-stretch and the applied electric displacement as demonstrated in Table 3.2. Therefore, it is revealed that both the mechanical and the electrical loads could modify the properties of DE medium, leading to the alteration of the characteristics of Rayleigh-Lamb wave propagation.

Figs. 3.9a to 3.9c demonstrate the effect of electrical load on the dispersion relations through the variation of the normalized phase velocity \hat{c} , the normalized wave frequency $\hat{\omega}$, and the normalized group velocity \hat{V}_G with the wavenumber for a viscous DE layer when $K(\hat{t}) = 0.9$, $\chi = 0.8$, and $\lambda = 1.5$. The solid and dashed curves represent the symmetric and antisymmetric modes, respectively. With regard to the symmetric mode, the phase velocity in the limit of long waves ($\hat{k} \rightarrow 0$) increases monotonically with the applied electric displacement. While a reverse trend is observed in the limit of short waves ($\hat{k} \rightarrow \infty$), i.e., the surface wave velocity decreases with the applied electrical load. This is caused by the reduction of the tension induced by the applied electrical load since the DE layer is fixed at the ends to maintain the pre-stretch. Interestingly, it is found that further increasing the electric displacement induces further reduction of the tension in the DE layer until the surface waves decays to zero, which is corresponding to the loss of surface stability. A similar phenomenon was also observed for the wave propagation in a purely elastic medium (Shmuel et al., 2012). The value of the applied electric displacement associated with the vanishing phase velocity can be perceived as a threshold \hat{d}_{th} at which the surface instability occurs. Such a threshold value depends on the pre-stretch, the material viscoelasticity and the relaxation status of the medium. Numerical results

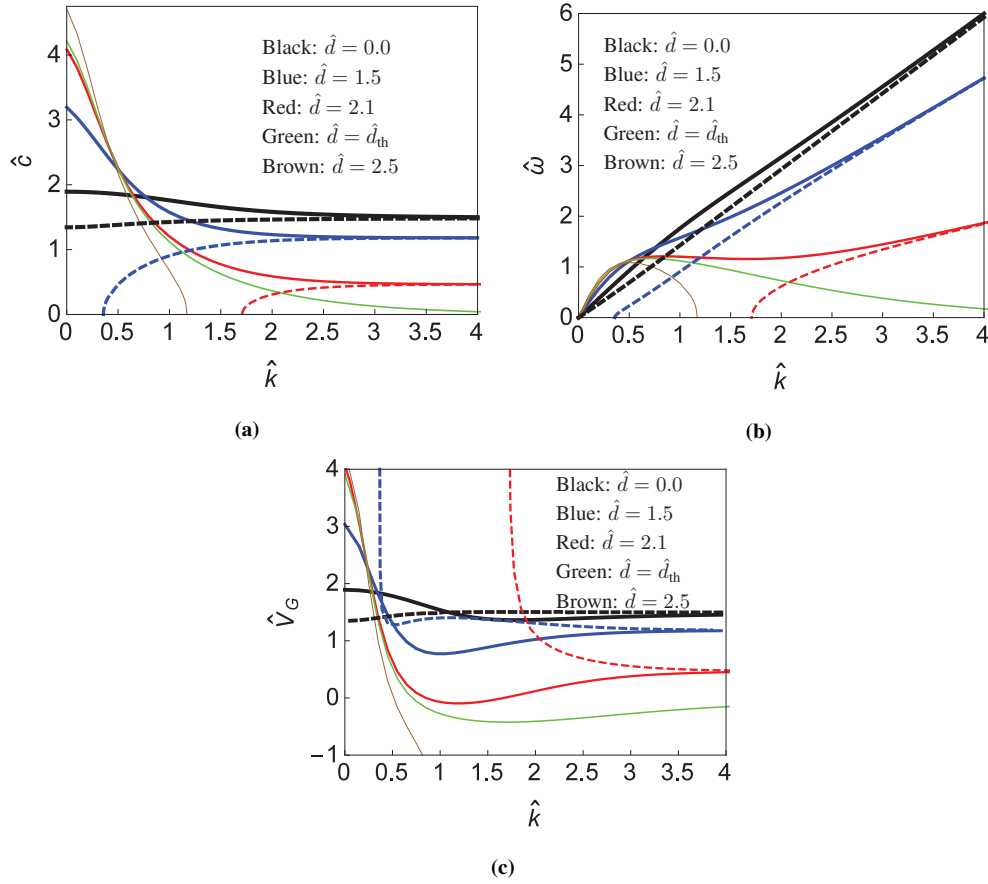


Figure 3.9: Effect of electrical load on the wave dispersion (a) normalized phase velocity, (b) normalized wave frequency, and (c) normalized group velocity for a pre-stretched viscous DE layer ($K(\hat{t}) = 0.9$, $\chi = 0.8$ and $\lambda = 1.5$). The continuous and dashed curves correspond to the symmetric mode and the antisymmetric mode, respectively.

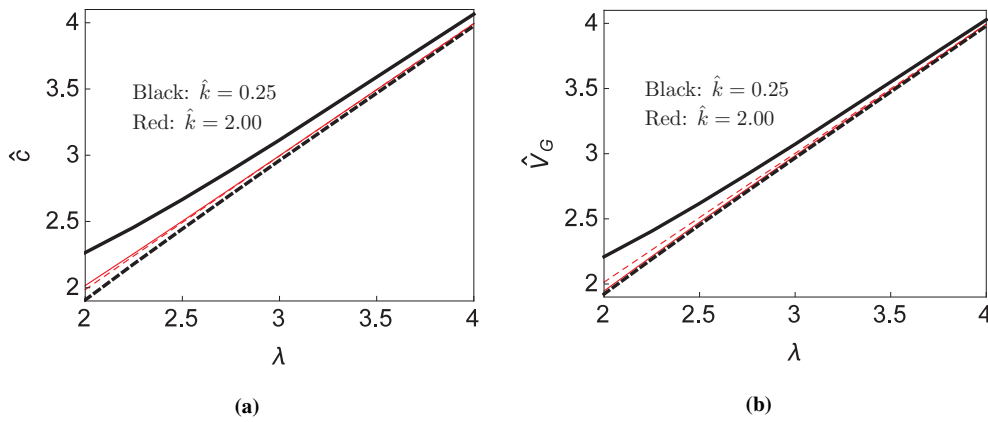


Figure 3.10: Variation of (a) phase velocity and (b) group velocity with respect to pre-stretch ratio λ ($\hat{d} = 0.5$, $\chi = 0.8$, and $K(\hat{t}) = 0.9$).

(a)				(b)			
λ	χ	$K(\hat{t})$	\hat{d}_{th}	λ	$K(\hat{t})$	χ	\hat{d}_{th}
1.25	0.6	0.7	2.091	1.5	0.7	0.4	2.252
		0.8	2.033			0.6	2.233
		0.9	1.985			0.8	2.216
		1.0	1.947			1.0	2.181
1.5	0.8	0.7	2.216	2.0	0.6	0.4	2.645
		0.8	2.196			0.6	2.636
		0.9	2.185			0.8	2.627
		1.0	2.181			1.0	2.622

(c)			
$K(\hat{t})$	χ	λ	\hat{d}_{th}
0.9	0.6	1.25	1.985
		1.50	2.188
		1.75	2.377
		2.00	2.583
0.8	0.8	1.25	1.972
		1.50	2.196
		1.75	2.399
		2.00	2.605

Table 3.3: Effect of (a) material relaxation status $K(\hat{t})$, (b) material viscosity χ , and (c) pre-stretch λ , on the threshold of the electric displacement \hat{d}_{th} .

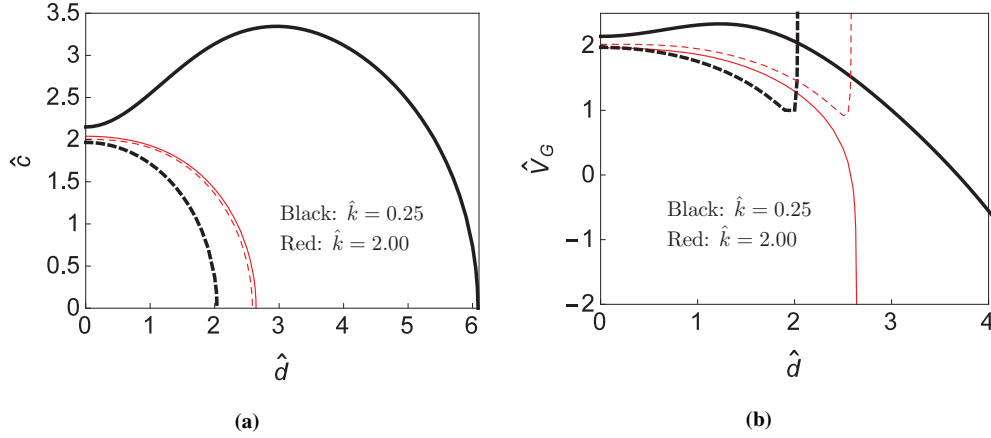


Figure 3.11: Variation of (a) phase velocity and (b) group velocity with respect to electric displacement \hat{d} ($\lambda = 2$, $\chi = 0.8$, and $K(\hat{t}) = 0.9$).

of this threshold value \hat{d}_{th} are listed in Table 3.3. A general trend is observed from Tables 3.3a and 3.3b that \hat{d}_{th} decreases with the relaxation status $K(\hat{t})$ while increases with the material viscoelasticity χ , which means that the material viscosity can hinder the loss of surface stability. However, such an effect from the material viscosity attenuates with the increase of the pre-stretch. Similar to the wave propagation in a purely elastic medium (Shmuel et al., 2012), it is found from Table 3.3c that the threshold value \hat{d}_{th} increases monotonically with the pre-stretch ratio λ , revealing a stabilizing effect of the pre-stretch. When the applied electric displacement $\hat{d} > \hat{d}_{\text{th}}$, for example, $\hat{d} = 2.5$ in Fig. 3.9a, it is observed that the phase velocity vanishes at a cut-off wavenumber denoted by $\hat{k}_{\text{cr}}^{\text{sym}}$, suggesting that there exists a critical wavelength, below which no symmetric mode wave can propagate through the DE medium.

For the antisymmetric mode, the phase velocity decreases with the increasing of the applied electric displacement \hat{d} as shown in Fig. 3.9a. It decays to zero at various cut-off wavenumbers, below which there is no propagation of longer antisymmetric mode waves. Such a wavenumber is denoted as $\hat{k}_{\text{cr}}^{\text{anti}}$, which increases with the applied electric displacement until it reaches the threshold value \hat{d}_{th} , at which $\hat{k}_{\text{cr}}^{\text{anti}} \rightarrow \infty$. It means when the applied electric displacement $\hat{d} > \hat{d}_{\text{th}}$, there is no propagation of any antisymmetric mode waves in the DE medium. It is the reason that there is only one symmetric mode for longer waves when the applied electric

displacement $\hat{d} = 2.5$ as shown in Figs. 3.9a and 3.9b shows the dispersion relation through the normalized wave frequencies versus the normalized wavenumber. For the antisymmetric mode, the normalized frequency increases monotonically with the normalized wavenumber. Considering the symmetric mode, one can find that when the applied electric field is low, a monotonic rise in the frequency with the increase of the wave number \hat{k} is observed. However, when the applied electric displacement \hat{d} is higher than a certain value, the normalized wave frequency curve becomes non-monotonic. The non-monotonicity of the symmetric mode indicates the possible existence of more than one wavenumber satisfying the dispersion relation. It means that as the frequency rises up, it is possible to have a shorter and slower wave accompanying the propagation of the longer and faster wave. Considering antisymmetric mode of group velocity in Fig. 3.9c, it is obvious that at $\hat{k} = \hat{k}_{co}^{anti}$, the group velocity becomes infinite, i.e., $\hat{V}_G \rightarrow \infty$.

Figs. 3.10 and 3.11, respectively, depict how the phase and group velocities are affected by the applied electromechanical loads (by changing λ and \hat{d}). As shown in Fig. 3.10, both the phase and the group velocities increase monotonically with the pre-stretch ratio λ of the DE layer for the waves with different wavenumber of \hat{k} . On the other hand, the effect of the electric displacement on the wave propagation speed is more complex as shown in Figs. 3.11a and 3.11b. It may increase or decrease the propagation speed depending on the wavenumber or the type of wave mode. The increase of the applied electric displacement induces more tension reduction in the medium, leading to the loss of the surface stability as demonstrated by the vanishing value of the phase velocity in Fig. 3.11a. Considering the antisymmetric mode, the phase velocity decreases as the electric displacement \hat{d} increases as shown in Fig. 3.11a. When the loss of surface stability of the DE layer occurs, only the antisymmetric mode wave within certain wavelength can propagate. With regard to the group velocity in Fig. 3.11b, as the electric displacement \hat{d} increases, it first decreases then rises up suddenly due to the loss of surface stability. The value of this group velocity is physically meaningless since there is no propagation of the wave with this particular wavenumber. On the other hand, regarding the

symmetric mode, for a long wave with small wave number ($\hat{k} = 0.25$ for example), both the phase and the group velocities first increases with any increase in the applied electric displacement \hat{d} and reaches a maximum value. Right after a certain electric displacement, the slope of the curve becomes negative and the velocities gradually decrease by any rise of the electric displacement \hat{d} . However, for the short waves with large wave number ($\hat{k} = 2$ for example), the applied electric displacement makes the wave propagate slower.

3.4 Conclusions

By studying the dispersion relations of a Rayleigh-Lamb wave propagating in a dielectric elastomer (DE) layer, this work aims to provide an increased understanding of the electroelastic dynamics subject, and uncover possible approaches to manipulate active waveguide applications of dielectric elastomers. Based on the finite-deformation viscoelasticity theory for dielectric elastomers, the wave motion equations are formulated according to the framework of small-amplitude wave propagation superposed on a finitely deformed DE layer. Simulation results have demonstrated the effects of material viscoelasticity, mechanical pre-stretch and applied electric load upon the wave dispersion relations for both the symmetric and antisymmetric wave modes. It is revealed that waves with certain frequencies could be filtered by the applied electrical load, suggesting that dielectric elastomers can be used as waveguides by actively tuning the applied electrical load. It is interesting to notice that the material viscoelasticity has no effect on the propagation of a symmetric mode wave with certain wavenumber, which is contingent on the applied electrical load as well. This finding provides insights in eliminating the material viscoelasticity effect on wave propagation by applying an electrical load. To the best knowledge of the authors, it is the first time to find that the Rayleigh-Lamb wave becomes non-dispersive in a DE medium with certain material viscoelasticity, and such a material viscoelasticity depends on the applied electromechanical loads. It again concludes

that both mechanical and electrical loads can change the wave propagation characteristics in the DE medium. This work is expected to provide guidance for the DE waveguide applications, particularly when the material viscoelasticity is involved.

Chapter 4

Contributions, Conclusions, and Future Work

4.1 Thesis contributions and conclusions

As a family of smart materials, dielectric elastomers (DEs) have received growing interest as alternatives to traditional piezoelectric ceramics in transduction technologies due to their unique properties, particularly large deformation capability. Better exploitation of these novel materials requires increased understanding on the fundamentals governing their delicate multi-physics coupling mechanisms. Despite the development of theories for finite electroelasticity, dynamic analysis on finitely deformed DEs is still very limited in the literature, mainly due to the complexity of the problems coupling electromechanical dynamics and material viscoelasticity. This thesis aims to tackle these challenges by developing rigorous modeling and simulation approaches for characterizing the Rayleigh-Lamb wave propagation in DE media. We expect that this research can contribute to provide a guideline for the design of active waveguide applications of dielectric elastomers, and close such a knowledge gap to certain extent.

The major contributions of the thesis include:

- (1) It is the first time in the literature that the wave propagation in a dielectric medium is formulated with the incorporation of material viscoelasticity, electromechanical coupling, and finite deformation. Novel solution technique has been proposed to derive the dispersion relations for electroelastic waves.
- (2) A comprehensive analysis has been conducted to identify what factors will affect the wave propagation in the DE medium from theoretical perspective, suggesting possible routes for actively manipulating DE waveguide. Some interesting findings are very useful for waveguide applications of dielectric elastomers, which could provide increased understanding on the electroelastic wave propagation in viscoelastic media.

Based on our modeling framework and simulation results, some concluding remarks of the thesis are listed below:

- (1) Based on the finite-deformation viscoelasticity model for dielectric elastomers, the small-amplitude wave propagation in a finitely deformed DE medium is investigated through the dispersion relations.
- (2) It is revealed that waves with certain frequencies could be filtered by the applied electric load, suggesting that dielectric elastomers can be used as waveguides by actively tuning the applied electric load.
- (3) It is found that the material viscosity has no effect on the propagation of symmetric mode wave with certain wavenumber, which could be adjusted by the applied electric load. This finding provides an insight in eliminating the material viscoelasticity effect on wave propagation by applying an electric load.
- (4) To the best knowledge of the author, it is the first time to find that the Rayleigh-Lamb

wave becomes non-dispersive in a DE medium with certain material viscoelasticity, and such a material viscoelasticity depends on the applied electromechanical loads.

4.2 Suggestions for future work

The results of this work are expected to be helpful for predicting the performance of DE waveguide devices and benefit their optimal design. However, this is a preliminary study to consider the material viscosity of DEs for the problems of electroelastic wave propagation. The general framework of this work can be adopted to study the problems of electroelastic wave propagation through DE media with different configurations according to particular applications. It should be noted that the challenge also comes from the complexity of the mathematical formulation behind, which makes the problem very difficult to be solved. Thus, the following suggestions are offered to be addressed in the future:

- (1) For the current simple configuration of DE waveguide, the effects of electromechanical loading routes should be further investigated. For example, the mechanical stretch could vary during the wave propagation.
- (2) In the current work it is assumed that the DE layer is a homogeneous medium. One can also examine the problems of wave propagation through inhomogeneous DE media or homogeneous DE media with different configurations, including periodic layered DE medium, fiber-reinforced DE medium, and tubular DE for example. Further knowledge from these studies will promote the development of DE-based metastructures for active waveguide applications.
- (3) The framework for wave propagation formulation in this thesis is limited to the small-amplitude wave propagation. Hence the problems of finite-amplitude wave propagation through viscous DE media are still remained unsolved, which could be a future direction.

Bibliography

Achenbach, J. D. and Reddy, D. P. (1967), ‘Note on wave propagation in linearly viscoelastic media’, *Zeitschrift für angewandte Mathematik und Physik ZAMP* **18**(1), 141–144.

Alleyen, D. (1997), ‘Long range propagation of lamb wave in chemical plant pipe-work’, *Materials Evaluation* pp. 504–508.

Alleyne, D. N. (1991), The nondestructive testing of plates using ultrasonic Lamb waves, PhD thesis, Department of Mechanical Engineering, Imperial College.

Araromi, O. and Gavrilovich, I. (2014a), ‘Rollable multisegment dielectric elastomer minimum energy structures for a deployable microsatellite gripper’, *IEEE/ASME Transactions on Mechatronics* **20**(1), 438–446.

Araromi, O. and Gavrilovich, I. (2014b), Towards a deployable satellite gripper based on multisegment dielectric elastomer minimum energy structures, in ‘Electroactive Polymer Actuators and Devices (EAPAD) 2014’, Vol. 9056, International Society for Optics and Photonics, p. 90562G.

Arruda, E. M. and Boyce, M. C. (1993), ‘A three-dimensional constitutive model for the large stretch behavior of rubber elastic materials’, *Journal of the Mechanics and Physics of Solids* **41**(2), 389–412.

Bai, Y., Jiang, Y., Chen, B., Chiang Foo, C., Zhou, Y., Xiang, F., Zhou, J., Wang, H. and

- Suo, Z. (2014), 'Cyclic performance of viscoelastic dielectric elastomers with solid hydrogel electrodes', *Applied Physics Letters* **104**(6), 062902.
- Barnett, D. and Lothe, J. (1985), 'Free surface (rayleigh) waves in anisotropic elastic half-spaces: the surface impedance method', *Proceedings of the Royal Society of London. A. Mathematical and Physical Sciences* **402**(1822), 135–152.
- Beatty, K. S. and Schmitt, D. R. (2003), 'Repeatability of multimode rayleigh-wave dispersion studies rayleigh-wave dispersion', *Geophysics* **68**(3), 782–790.
- Bergström, J. and Boyce, M. (2000), 'Large strain time-dependent behavior of filled elastomers', *Mechanics of materials* **32**(11), 627–644.
- Biggs, S. J. and Hitchcock, R. N. (2010), Artificial muscle actuators for haptic displays: system design to match the dynamics and tactile sensitivity of the human fingerpad, in 'Electroactive Polymer Actuators and Devices (EAPAD) 2010', Vol. 7642, International Society for Optics and Photonics, p. 76420I.
- Bilodeau, R. A., White, E. L. and Kramer, R. K. (2015), Monolithic fabrication of sensors and actuators in a soft robotic gripper, in '2015 IEEE/RSJ International Conference on Intelligent Robots and Systems (IROS)', IEEE, pp. 2324–2329.
- Bonwit, N., Heim, J., Rosenthal, M., Duncheon, C. and Beavers, A. (2006), Design of commercial applications of epam technology, in 'Smart Structures and Materials 2006: Electroactive Polymer Actuators and Devices (EAPAD)', Vol. 6168, International Society for Optics and Photonics, p. 616805.
- Boyce, M. C. and Arruda, E. M. (2000), 'Constitutive models of rubber elasticity: a review', *Rubber chemistry and technology* **73**(3), 504–523.
- Brochu, P. and Pei, Q. (2010), 'Advances in dielectric elastomers for actuators and artificial muscles', *Macromolecular rapid communications* **31**(1), 10–36.

- Brochu, P., Yuan, W., Zhang, H. and Pei, Q. (2009), Dielectric elastomers for direct wind-to-electricity power generation, in 'ASME 2009 Conference on Smart Materials, Adaptive Structures and Intelligent Systems', American Society of Mechanical Engineers Digital Collection, pp. 197–204.
- Buchen, P. W. (1971), 'Plane waves in linear viscoelastic media', *Geophysical Journal International* **23**(5), 531–542.
- Caldwell, D. G., Tsagarakis, N. and Medrano-Cerda, G. (2000), 'Bio-mimetic actuators: polymeric pseudo muscular actuators and pneumatic muscle actuators for biological emulation', *Mechatronics* **10**(4-5), 499–530.
- Campbell, C. (1998), *Surface Acoustic Wave Devices for Mobile and Wireless Communications, Four-Volume Set*, Academic press.
- Carcione, J. M., Kosloff, D. and Kosloff, R. (1988), 'Wave propagation simulation in a linear viscoelastic medium', *Geophysical Journal International* **95**(3), 597–611.
- Carpi, F., Bauer, S. and De Rossi, D. (2010), 'Stretching dielectric elastomer performance', *Science* **330**(6012), 1759–1761.
- Carpi, F., De Rossi, D., Kornbluh, R., Pelrine, R. E. and Sommer-Larsen, P. (2011), *Dielectric elastomers as electromechanical transducers: Fundamentals, materials, devices, models and applications of an emerging electroactive polymer technology*, Elsevier.
- Carpi, F. and Frediani, G. (2011), 'Bioinspired tunable lens with muscle-like electroactive elastomers', *Advanced functional materials* **21**(21), 4152–4158.
- Carpi, F., Frediani, G. and De Rossi, D. (2009), 'Hydrostatically coupled dielectric elastomer actuators', *IEEE/ASME Transactions On Mechatronics* **15**(2), 308–315.
- Chiba, S., Waki, M., Kornbluh, R. and Pelrine, R. (2008), Innovative power generators for energy harvesting using electroactive polymer artificial muscles, in 'Electroactive Polymer

- Actuators and Devices (EAPAD) 2008', Vol. 6927, International Society for Optics and Photonics, p. 692715.
- Chiba, S., Waki, M., Wada, T., Hirakawa, Y., Masuda, K. and Ikoma, T. (2013), 'Consistent ocean wave energy harvesting using electroactive polymer (dielectric elastomer) artificial muscle generators', *Applied energy* **104**, 497–502.
- Chimenti, D. and Martin, R. (1991), 'Nondestructive evaluation of composite laminates by leaky lamb waves', *Ultrasonics* **29**(1), 13–21.
- Chimenti, D. and Nayfeh, A. H. (1990), 'Ultrasonic reflection and guided wave propagation in biaxially laminated composite plates', *The Journal of the Acoustical Society of America* **87**(4), 1409–1415.
- Cho, Y. (2000), 'Estimation of ultrasonic guided wave mode conversion in a plate with thickness variation', *IEEE transactions on ultrasonics, ferroelectrics, and frequency control* **47**(3), 591–603.
- Christensen, R. (1980), 'A nonlinear theory of viscoelasticity for application to elastomers', *Journal of Applied Mechanics* **47**(4), 762–768.
- Coquin, G. (1964), 'Attenuation of guided waves in isotropic viscoelastic materials', *The Journal of the Acoustical Society of America* **36**(6), 1074–1080.
- Coury, A. J., Slaikeu, P. C., Cahalan, P. T., Stokes, K. B. and Hobot, C. M. (1988), 'Factors and interactions affecting the performance of polyurethane elastomers in medical devices', *Journal of biomaterials applications* **3**(2), 130–179.
- Datta, S. K., Shah, A., Karunasena, W., Olsson, P. and Boström, A. (1990), 'Wave propagation in the presence of interface layers in composites', *Materials Science and Engineering: A* **126**(1-2), 141–147.

- Destrade, M., Ogden, R. W. and Saccomandi, G. (2009), 'Small amplitude waves and stability for a pre-stressed viscoelastic solid', *Zeitschrift für angewandte Mathematik und Physik* **60**(3), 511–528.
- Destrade, M. and Saccomandi, G. (2004), 'Finite-amplitude inhomogeneous waves in mooney–rivlin viscoelastic solids', *Wave Motion* **40**(3), 251–262.
- Destrade, M. and Saccomandi, G. (2005), 'Finite amplitude elastic waves propagating in compressible solids', *Physical Review E* **72**(1), 016620.
- Ditri, J. J. (1994), 'Utilization of guided elastic waves for the characterization of circumferential cracks in hollow cylinders', *The Journal of the Acoustical Society of America* **96**(6), 3769–3775.
- Dorfmann, A. and Ogden, R. (2005), 'Nonlinear electroelasticity', *Acta Mechanica* **174**(3–4), 167–183.
- Dorfmann, A. and Ogden, R. W. (2010), 'Electroelastic waves in a finitely deformed electroactive material', *IMA Journal of Applied Mathematics* **75**(4), 603–636.
- Drozdov, A. D. (1997), 'A constitutive model for nonlinear viscoelastic media', *International Journal of Solids and Structures* **34**(21), 2685–2707.
- Duduta, M., Clarke, D. R. and Wood, R. J. (2017), A high speed soft robot based on dielectric elastomer actuators, in '2017 IEEE International Conference on Robotics and Automation (ICRA)', IEEE, pp. 4346–4351.
- Eguchi, M. (1925), 'Xx. on the permanent electret', *The London, Edinburgh, and Dublin Philosophical Magazine and Journal of Science* **49**(289), 178–192.
- Eringen, A. C. (1963), 'On the foundations of electroelastostatics', *International Journal of Engineering Science* **1**(1), 127–153.

- Eringen, A. and Maugin, G. (1989), 'Electrodynamics of continua, vols i, ii'.
- Flory, P. J. and Rehner Jr, J. (1943), 'Statistical mechanics of cross-linked polymer networks i. rubberlike elasticity', *The journal of chemical physics* **11**(11), 512–520.
- Foo, C., Jin Adrian Koh, S., Keplinger, C., Kaltseis, R., Bauer, S. and Suo, Z. (2012), 'Performance of dissipative dielectric elastomer generators', *Journal of Applied Physics* **111**(9), 094107.
- Fox, J. and Goulbourne, N. (2008), 'On the dynamic electromechanical loading of dielectric elastomer membranes', *Journal of the Mechanics and Physics of Solids* **56**(8), 2669–2686.
- Fox, J. and Goulbourne, N. (2009), 'Electric field-induced surface transformations and experimental dynamic characteristics of dielectric elastomer membranes', *Journal of the Mechanics and Physics of Solids* **57**(8), 1417–1435.
- Galán, J. M. and Abascal, R. (2002), 'Numerical simulation of lamb wave scattering in semi-infinite plates', *International Journal for Numerical Methods in Engineering* **53**(5), 1145–1173.
- Galich, P. I. and Rudykh, S. (2016), 'Manipulating pressure and shear waves in dielectric elastomers via external electric stimuli', *International Journal of Solids and Structures* **91**, 18–25.
- Galich, P. I. and Rudykh, S. (2017), 'Shear wave propagation and band gaps in finitely deformed dielectric elastomer laminates: long wave estimates and exact solution', *Journal of Applied Mechanics* **84**(9), 091002.
- Gei, M., Roccabianca, S. and Bacca, M. (2010), 'Controlling bandgap in electroactive polymer-based structures', *IEEE/ASME Transactions on Mechatronics* **16**(1), 102–107.
- Gent, A. (1996), 'A new constitutive relation for rubber', *Rubber chemistry and technology* **69**(1), 59–61.

- Godaba, H., Wang, Y., Cao, J. and Zhu, J. (2016), Development of soft robots using dielectric elastomer actuators, in 'Electroactive Polymer Actuators and Devices (EAPAD) 2016', Vol. 9798, International Society for Optics and Photonics, p. 97981T.
- Gravenkamp, H., Song, C. and Prager, J. (2012a), 'A numerical approach for the computation of dispersion relations for plate structures using the scaled boundary finite element method', *Journal of sound and vibration* **331**(11), 2543–2557.
- Gravenkamp, H., Song, C. and Prager, J. (2012b), 'A numerical approach for the computation of dispersion relations for plate structures using the scaled boundary finite element method', *Journal of sound and vibration* **331**(11), 2543–2557.
- Green, M. and Tobolsky, A. (1946), 'A new approach to the theory of relaxing polymeric media', *The Journal of Chemical Physics* **14**(2), 80–92.
- Gueraud, R., Noel-Leroux, J.-P., Livolant, M. and Michalopoulos, A. (1985), 'Seismic isolation using sliding-elastomer bearing pads', *Nuclear Engineering and Design* **84**(3), 363–377.
- Ha, S. M., Yuan, W., Pei, Q., Pelrine, R. and Stanford, S. (2006), 'Interpenetrating polymer networks for high-performance electroelastomer artificial muscles', *Advanced Materials* **18**(7), 887–891.
- Hayes, M. A. and Saccomandi, G. (2000), 'Finite amplitude transverse waves in special incompressible viscoelastic solids', *Journal of elasticity and the physical science of solids* **59**(1-3), 213–225.
- Hayes, M. A. and Saccomandi, G. (2002), 'Finite amplitude waves superimposed on pseudo-planar motions for mooney–rivlin viscoelastic solids', *International journal of non-linear mechanics* **37**(7), 1139–1146.
- Hayes, M. and Rivlin, R. (1969), 'Propagation of sinusoidal small-amplitude waves in a de-

- formed viscoelastic solid. i', *The Journal of the Acoustical Society of America* **46**(3B), 610–616.
- Hayes, M. and Rivlin, R. (1972), 'Propagation of sinusoidal small-amplitude waves in a deformed viscoelastic solid. ii', *The Journal of the Acoustical Society of America* **51**(5B), 1652–1663.
- Heng, K.-R., Ahmed, A. S., Shrestha, M. and Lau, G.-K. (2017), Strong dielectric-elastomer grippers with tension arch flexures, in 'Electroactive Polymer Actuators and Devices (EAPAD) 2017', Vol. 10163, International Society for Optics and Photonics, p. 101631Z.
- Hensel, P. C. and Gillings, G. W. (1986), 'Dielectric optical waveguide connecting device'. US Patent 4,575,182.
- Heydt, R., Kornbluh, R., Eckerle, J. and Pelrine, R. (2006), Sound radiation properties of dielectric elastomer electroactive polymer loudspeakers, in 'Smart Structures and Materials 2006: Electroactive Polymer Actuators and Devices (EAPAD)', Vol. 6168, International Society for Optics and Photonics, p. 61681M.
- Hong, W. (2011), 'Modeling viscoelastic dielectrics', *Journal of the Mechanics and Physics of Solids* **59**(3), 637–650.
- Hoummady, M., Campitelli, A. and Wlodarski, W. (1997), 'Acoustic wave sensors: design, sensing mechanisms and applications', *Smart materials and structures* **6**(6), 647.
- Huang, J., Shian, S., Suo, Z. and Clarke, D. R. (2013), 'Maximizing the energy density of dielectric elastomer generators using equi-biaxial loading', *Advanced Functional Materials* **23**(40), 5056–5061.
- Huang, R. and Suo, Z. (2011), 'Electromechanical phase transition in dielectric elastomers', *Proceedings of the Royal Society A: Mathematical, Physical and Engineering Sciences* **468**(2140), 1014–1040.

- Ionov, L. (2014), 'Polymeric actuators', *Langmuir* **31**(18), 5015–5024.
- Jin, B., Lee, J.-H., Zhou, Z., Zhang, G., Lee, G.-B., Ren, H. and Nah, C. (2016), 'Adaptive liquid lens driven by elastomer actuator', *Optical Engineering* **55**(1), 017107.
- Jung, K., Kim, K. J. and Choi, H. R. (2008), 'A self-sensing dielectric elastomer actuator', *Sensors and Actuators A: Physical* **143**(2), 343–351.
- Kaliske, M. and Rotherth, H. (1997), 'Formulation and implementation of three-dimensional viscoelasticity at small and finite strains', *Computational Mechanics* **19**(3), 228–239.
- Karsten, R., Flittner, K., Haus, H. and Schlaak, H. F. (2013), Development of an active isolation mat based on dielectric elastomer stack actuators for mechanical vibration cancellation, in 'Electroactive Polymer Actuators and Devices (EAPAD) 2013', Vol. 8687, International Society for Optics and Photonics, p. 86870Y.
- Keong, G.-K., La, T.-G., Shiau, L.-L. and Tan, A. W. Y. (2014), Challenges of using dielectric elastomer actuators to tune liquid lens, in 'Electroactive Polymer Actuators and Devices (EAPAD) 2014', Vol. 9056, International Society for Optics and Photonics, p. 90561J.
- Keplinger, C., Kaltenbrunner, M., Arnold, N. and Bauer, S. (2010), 'Röntgen's electrode-free elastomer actuators without electromechanical pull-in instability', *Proceedings of the National Academy of Sciences* **107**(10), 4505–4510.
- Kikuchi, M. and Aiken, I. D. (1997), 'An analytical hysteresis model for elastomeric seismic isolation bearings', *Earthquake engineering & structural dynamics* **26**(2), 215–231.
- Kim, S., Laschi, C. and Trimmer, B. (2013), 'Soft robotics: a bioinspired evolution in robotics', *Trends in biotechnology* **31**(5), 287–294.
- Knoop, L. E. and Rossiter, J. (2014), Towards shear tactile displays with deas, in 'Electroactive Polymer Actuators and Devices (EAPAD) 2014', Vol. 9056, International Society for Optics and Photonics, p. 905610.

- Kofod, G., Sommer-Larsen, P., Kornbluh, R. and Pelrine, R. (2003), 'Actuation response of polyacrylate dielectric elastomers', *Journal of intelligent material systems and structures* **14**(12), 787–793.
- Kofod, G., Wirges, W., Paajanen, M. and Bauer, S. (2007), 'Energy minimization for self-organized structure formation and actuation', *Applied Physics Letters* **90**(8), 081916.
- Koh, S. J. A., Li, T., Zhou, J., Zhao, X., Hong, W., Zhu, J. and Suo, Z. (2011), 'Mechanisms of large actuation strain in dielectric elastomers', *Journal of Polymer Science Part B: Polymer Physics* **49**(7), 504–515.
- Koh, S. J. A., Zhao, X. and Suo, Z. (2009), 'Maximal energy that can be converted by a dielectric elastomer generator', *Applied Physics Letters* **94**(26), 262902.
- Kollosche, M., Kofod, G., Suo, Z. and Zhu, J. (2015), 'Temporal evolution and instability in a viscoelastic dielectric elastomer', *Journal of the Mechanics and Physics of Solids* **76**, 47–64.
- Kornbluh, R. D., Pelrine, R. E., Prahlad, H., Chiba, S., Eckerle, J. S., Chavez, B., Stanford, S. E. and Low, T. (2009), 'Wave powered generation using electroactive polymers'. US Patent 7,557,456.
- Kornbluh, R. D., Pelrine, R., Pei, Q., Heydt, R., Stanford, S., Oh, S. and Eckerle, J. (2002), Electroelastomers: applications of dielectric elastomer transducers for actuation, generation, and smart structures, in 'Smart Structures and Materials 2002: Industrial and Commercial Applications of Smart Structures Technologies', Vol. 4698, International Society for Optics and Photonics, pp. 254–270.
- Kornbluh, R. D., Pelrine, R., Prahlad, H., Wong-Foy, A., McCoy, B., Kim, S., Eckerle, J. and Low, T. (2012a), 'Dielectric elastomers: Stretching the capabilities of energy harvesting', *MRS bulletin* **37**(3), 246–253.

- Kornbluh, R. D., Pelrine, R., Prahlad, H., Wong-Foy, A., McCoy, B., Kim, S., Eckerle, J. and Low, T. (2012*b*), From boots to buoys: promises and challenges of dielectric elastomer energy harvesting, *in* 'Electroactivity in polymeric materials', Springer, pp. 67–93.
- Kumar, M., Whittaker, A. S. and Constantinou, M. C. (2014), 'An advanced numerical model of elastomeric seismic isolation bearings', *Earthquake Engineering & Structural Dynamics* **43**(13), 1955–1974.
- Lai, H., Tan, C. A. and Xu, Y. (2011), Dielectric elastomer energy harvesting and its application to human walking, *in* 'ASME 2011 International Mechanical Engineering Congress and Exposition', American Society of Mechanical Engineers Digital Collection, pp. 601–607.
- Lamb, H. (1917), 'On waves in an elastic plate', *Proceedings of the Royal Society of London. Series A, Containing papers of a mathematical and physical character* **93**(648), 114–128.
- Lau, G.-K., Heng, K.-R., Ahmed, A. S. and Shrestha, M. (2017), 'Dielectric elastomer fingers for versatile grasping and nimble pinching', *Applied Physics Letters* **110**(18), 182906.
- Lau, G.-K., Lim, H.-T., Teo, J.-Y. and Chin, Y.-W. (2014), 'Lightweight mechanical amplifiers for rolled dielectric elastomer actuators and their integration with bio-inspired wing flappers', *Smart Materials and Structures* **23**(2), 025021.
- Lee, B. and Staszewski, W. (2003), 'Modelling of lamb waves for damage detection in metallic structures: Part i. wave propagation', *Smart Materials and Structures* **12**(5), 804.
- Lee, H. S., Phung, H., Lee, D.-H., Kim, U. K., Nguyen, C. T., Moon, H., Koo, J. C., Choi, H. R. et al. (2014), 'Design analysis and fabrication of arrayed tactile display based on dielectric elastomer actuator', *Sensors and Actuators A: Physical* **205**, 191–198.
- Leeper, H. M. and Wright, R. M. (1983), 'Elastomers in medicine', *Rubber chemistry and technology* **56**(3), 523–556.

- Li, J. and Liu, L. (2019), 'Dielectric elastomer spring-roll bending actuators: applications in soft robotics and design', *Soft robotics* **6**(1), 69–81.
- Li, T., Qu, S. and Yang, W. (2012), 'Electromechanical and dynamic analyses of tunable dielectric elastomer resonator', *International Journal of Solids and Structures* **49**(26), 3754–3761.
- Li, Y., Zhou, J. and Jiang, L. (2019), 'Investigation on the dynamic performance of viscoelastic dielectric elastomer oscillators considering nonlinear material viscosity', *Journal of Intelligent Material Systems and Structures* p. 1045389X19880022.
- Lindner, G. (2008), 'Sensors and actuators based on surface acoustic waves propagating along solid–liquid interfaces', *Journal of Physics D: Applied Physics* **41**(12), 123002.
- Liu, Lei Chen, H. S. J. Z. J. W. Y. J. S. (2014), 'Experimental study on the dynamic response of in-plane deformation of dielectric elastomer under alternating electric load', *Smart Materials and Structures* **23**(2), 025037.
- Liu, Y., Liu, L., Zhang, Z., Jiao, Y., Sun, S. and Leng, J. (2010), 'Analysis and manufacture of an energy harvester based on a mooney-rivlin–type dielectric elastomer', *EPL (Europhysics Letters)* **90**(3), 36004.
- Löwe, C., Zhang, X. and Kovacs, G. (2005), 'Dielectric elastomers in actuator technology', *Advanced Engineering Materials* **7**(5), 361–367.
- Lowe, M., Alleyne, D. and Cawley, P. (1998), 'The mode conversion of a guided wave by a part-circumferential notch in a pipe', *Journal of Applied mechanics* **65**(3), 649–656.
- Lu, T., Huang, J., Jordi, C., Kovacs, G., Huang, R., Clarke, D. R. and Suo, Z. (2012), 'Dielectric elastomer actuators under equal-biaxial forces, uniaxial forces, and uniaxial constraint of stiff fibers', *Soft Matter* **8**(22), 6167–6173.
- Maugin, G. A. (1992), *Nonlinear electromechanical couplings*, John Wiley & Sons Incorporated.

- McKay, T., O'Brien, B., Calius, E. and Anderson, I. (2010), 'An integrated, self-priming dielectric elastomer generator', *Applied Physics Letters* **97**(6), 062911.
- McMillin, C. R. (1994), 'Elastomers for biomedical applications', *Rubber chemistry and technology* **67**(3), 417–446.
- Mockensturm, E. M. and Goulbourne, N. (2006), 'Dynamic response of dielectric elastomers', *International Journal of Non-Linear Mechanics* **41**(3), 388–395.
- Modjarrad, K. and Ebnesajjad, S. (2013), *Handbook of polymer applications in medicine and medical devices*, Elsevier.
- Mohabuth, M., Kotousov, A. and Ng, C.-T. (2019), 'Large acoustoelastic effect for lamb waves propagating in an incompressible elastic plate', *The Journal of the Acoustical Society of America* **145**(3), 1221–1229.
- Mooney, M. (1940), 'A theory of large elastic deformation', *Journal of applied physics* **11**(9), 582–592.
- Morgan, D. (2010), *Surface acoustic wave filters: With applications to electronic communications and signal processing*, Academic Press.
- Möbinger, H., Haus, H., Kauer, M. and Schlaak, H. F. (2014), Tactile feedback to the palm using arbitrarily shaped dea, in 'Electroactive Polymer Actuators and Devices (EAPAD) 2014', Vol. 9056, International Society for Optics and Photonics, p. 90563C.
- Nam, S., Yun, S., Yoon, J. W., Park, S., Park, S. K., Mun, S., Park, B. and Kyung, K.-U. (2018), 'A robust soft lens for tunable camera application using dielectric elastomer actuators', *Soft robotics* **5**(6), 777–782.
- Nguyen, N.-T., Ho, S.-S. and Low, C. L.-N. (2004), 'A polymeric microgripper with integrated thermal actuators', *Journal of Micromechanics and Microengineering* **14**(7), 969.

- Nicholson, P. H., Moilanen, P., Kärkkäinen, T., Timonen, J. and Cheng, S. (2002), 'Guided ultrasonic waves in long bones: modelling, experiment and in vivo application', *Physiological measurement* **23**(4), 755.
- O'Brien, B. M., Rosset, S., Shea, H. R. and Anderson, I. A. (2012), Cutting the fat: artificial muscle oscillators for lighter, cheaper, and slimmer devices, in 'Electroactive Polymer Actuators and Devices (EAPAD) 2012', Vol. 8340, International Society for Optics and Photonics, p. 834008.
- Ogden, R. W. (1972), 'Large deformation isotropic elasticity—on the correlation of theory and experiment for incompressible rubberlike solids', *Proc. R. Soc. Lond. A* **326**(1567), 565–584.
- Ohm, C., Brehmer, M. and Zentel, R. (2010), 'Liquid crystalline elastomers as actuators and sensors', *Advanced Materials* **22**(31), 3366–3387.
- Oliver, J. (1962), 'A summary of observed seismic surface wave dispersion', *Bulletin of the Seismological Society of America* **52**(1), 81–86.
- O'Halloran, A., O'malley, F. and McHugh, P. (2008), 'A review on dielectric elastomer actuators, technology, applications, and challenges', *Journal of Applied Physics* **104**(7), 9.
- Pagneux, V. and Maurel, A. (2001), 'Determination of lamb mode eigenvalues', *The Journal of the Acoustical Society of America* **110**(3), 1307–1314.
- Pao, Y.-H. (1978), Electromagnetic forces in deformable continua, in 'In: Mechanics today. Volume 4.(A78-35706 14-70) New York, Pergamon Press, Inc., 1978, p. 209-305. NSF-supported research.', Vol. 4, pp. 209–305.
- Park, H. S., Suo, Z., Zhou, J. and Klein, P. A. (2012), 'A dynamic finite element method for inhomogeneous deformation and electromechanical instability of dielectric elastomer transducers', *International Journal of Solids and Structures* **49**(15-16), 2187–2194.

- Park, S., Kim, H., Vosgueritchian, M., Cheon, S., Kim, H., Koo, J. H., Kim, T. R., Lee, S., Schwartz, G., Chang, H. et al. (2014), 'Stretchable energy-harvesting tactile electronic skin capable of differentiating multiple mechanical stimuli modes', *Advanced Materials* **26**(43), 7324–7332.
- Park, S., Park, B., Nam, S., Yun, S., Park, S. K., Mun, S., Lim, J. M., Ryu, Y., Song, S. H. and Kyung, K.-U. (2017), 'Electrically tunable binary phase fresnel lens based on a dielectric elastomer actuator', *Optics express* **25**(20), 23801–23808.
- Pei, Q., Rosenthal, M., Stanford, S., Prahlad, H. and Pelrine, R. (2004), 'Multiple-degrees-of-freedom electroelastomer roll actuators', *Smart materials and structures* **13**(5), N86.
- Pelrine, R. E., Kornbluh, R. D. and Joseph, J. P. (1998), 'Electrostriction of polymer dielectrics with compliant electrodes as a means of actuation', *Sensors and Actuators A: Physical* **64**(1), 77–85.
- Pelrine, R. and Kornbluh, R. (2000a), 'High-speed electrically actuated elastomers with strain greater than 100%', *Science* **287**(5454), 836–839.
- Pelrine, R. and Kornbluh, R. (2000b), 'High-strain actuator materials based on dielectric elastomers', *Advanced Materials* **12**(16), 1223–1225.
- Pelrine, R., Kornbluh, R. D., Eckerle, J., Jeuck, P., Oh, S., Pei, Q. and Stanford, S. (2001), Dielectric elastomers: generator mode fundamentals and applications, in 'Smart Structures and Materials 2001: Electroactive Polymer Actuators and Devices', Vol. 4329, International Society for Optics and Photonics, pp. 148–156.
- Pelrine, R., Kornbluh, R. D., Pei, Q., Stanford, S., Oh, S., Eckerle, J., Full, R. J., Rosenthal, M. A. and Meijer, K. (2002), Dielectric elastomer artificial muscle actuators: toward biomimetic motion, in 'Smart Structures and Materials 2002: Electroactive polymer actuators and devices (EAPAD)', Vol. 4695, International Society for Optics and Photonics, pp. 126–137.

- Pelrine, R., Kornbluh, R., Joseph, J., Heydt, R., Pei, Q. and Chiba, S. (2000), 'High-field deformation of elastomeric dielectrics for actuators', *Materials Science and Engineering: C* **11**(2), 89–100.
- Plante, J.-S. and Dubowsky, S. (2006), 'Large-scale failure modes of dielectric elastomer actuators', *International journal of solids and structures* **43**(25-26), 7727–7751.
- Plante, J.-S. and Dubowsky, S. (2007), 'On the performance mechanisms of dielectric elastomer actuators', *Sensors and Actuators A: Physical* **137**(1), 96–109.
- Rasti, P., Hous, H., Schlaak, H. F., Kiefer, R. and Anbarjafari, G. (2015), 'Dielectric elastomer stack actuator-based autofocus fluid lens', *Applied optics* **54**(33), 9976–9980.
- Rayleigh, L. (1885), 'On waves propagated along the plane surface of an elastic solid', *Proceedings of the London Mathematical Society* **1**(1), 4–11.
- Reese, S. (2003), 'A micromechanically motivated material model for the thermo-viscoelastic material behaviour of rubber-like polymers', *International Journal of Plasticity* **19**(7), 909–940.
- Reese, S. and Govindjee, S. (1998), 'A theory of finite viscoelasticity and numerical aspects', *International journal of solids and structures* **35**(26-27), 3455–3482.
- Rivlin, R. (1948a), 'Large elastic deformations of isotropic materials iv. further developments of the general theory', *Phil. Trans. R. Soc. Lond. A* **241**(835), 379–397.
- Rivlin, R. S. (1948b), 'The hydrodynamics of non-newtonian fluids. i', *Proceedings of the Royal Society of London. Series A. Mathematical and Physical Sciences* **193**(1033), 260–281.
- Romeo, M. (2001), 'Rayleigh waves on a viscoelastic solid half-space', *The Journal of the Acoustical Society of America* **110**(1), 59–67.

- Rosenthal and Pei (2008), ‘Rolled electroactive polymers’. US Patent App. 11/695,976.
- Saccomandi, G. (2005), ‘Small amplitude plane waves in deformed mooney—rivlin viscoelastic solids’, *Mathematics and mechanics of solids* **10**(4), 361–376.
- Sacerdote, M. (1899), ‘On the electrical deformation of isotropic dielectric solids’, *J. Phys* **3**, 282–285.
- Shankar, R., Ghosh, T. K. and Spontak, R. J. (2007), ‘Electroactive nanostructured polymers as tunable actuators’, *Advanced Materials* **19**(17), 2218–2223.
- Sharma, J. (2005), ‘Some considerations on the rayleigh–lamb wave propagation in viscothermoelastic plates’, *Modal Analysis* **11**(10), 1311–1335.
- Sharma, J. and Othman, M. I. (2007), ‘Effect of rotation on generalized thermo-viscoelastic rayleigh–lamb waves’, *International Journal of Solids and Structures* **44**(13), 4243–4255.
- Sheng, J., Chen, H., Li, B. and Chang, L. (2013), ‘Temperature dependence of the dielectric constant of acrylic dielectric elastomer’, *Applied Physics A* **110**(2), 511–515.
- Shian, S., Bertoldi, K. and Clarke, D. R. (2015), ‘Dielectric elastomer based “grippers” for soft robotics’, *Advanced Materials* **27**(43), 6814–6819.
- Shian, S., Diebold, R. M. and Clarke, D. R. (2013), ‘Tunable lenses using transparent dielectric elastomer actuators’, *Optics express* **21**(7), 8669–8676.
- Shian, S., Huang, J., Zhu, S. and Clarke, D. R. (2014), ‘Optimizing the electrical energy conversion cycle of dielectric elastomer generators’, *Advanced Materials* **26**(38), 6617–6621.
- Shintake, J., Cacucciolo, V., Shea, H. and Floreano, D. (2018), ‘Soft biomimetic fish robot made of dielectric elastomer actuators’, *Soft robotics* **5**(4), 466–474.
- Shmuel, G. (2013), ‘Electrostatically tunable band gaps in finitely extensible dielectric elastomer fiber composites’, *International Journal of Solids and Structures* **50**(5), 680–686.

- Shmuel, G. and deBotton, G. (2012), 'Band-gaps in electrostatically controlled dielectric laminates subjected to incremental shear motions', *Journal of the Mechanics and Physics of Solids* **60**(11), 1970–1981.
- Shmuel, G., Gei, M. et al. (2012), 'The rayleigh–lamb wave propagation in dielectric elastomer layers subjected to large deformations', *International Journal of Non-Linear Mechanics* **47**(2), 307–316.
- Shmuel, G. et al. (2013), 'Axisymmetric wave propagation in finitely deformed dielectric elastomer tubes', *Proc. R. Soc. A* **469**(2155), 20130071.
- Sidoroff, F. (1982), 'Incremental constitutive equation for large strain elasto plasticity', *International Journal of Engineering Science* **20**(1), 19–26.
- Simo, J. C. (1987), 'On a fully three-dimensional finite-strain viscoelastic damage model: formulation and computational aspects', *Computer methods in applied mechanics and engineering* **60**(2), 153–173.
- Sogabe, Y. and Tsuzuki, M. (1986), 'Identification of the dynamic properties of linear viscoelastic materials by the wave propagation testing', *Bulletin of JSME* **29**(254), 2410–2417.
- Song, Y.-Y., Castagna, J. P., Black, R. A. and Knapp, R. W. (1989), Sensitivity of near-surface shear-wave velocity determination from rayleigh and love waves, in 'SEG Technical Program Expanded Abstracts 1989', Society of Exploration Geophysicists, pp. 509–512.
- Sun, W., Liu, F., Ma, Z., Li, C. and Zhou, J. (2016), 'Soft mobile robots driven by foldable dielectric elastomer actuators', *Journal of Applied Physics* **120**(8), 084901.
- Suo, Z., Zhao, X. and Greene, W. H. (2008), 'A nonlinear field theory of deformable dielectrics', *Journal of the Mechanics and Physics of Solids* **56**(2), 467–486.
- Tal-Ezer, H., Carcione, J. and Kosloff, D. (1990), 'An accurate and efficient scheme for wave propagation in linear viscoelastic media', *Geophysics* **55**(10), 1366–1379.

- Taylor, A. W., Lin, A. N. and Martin, J. W. (1992), 'Performance of elastomers in isolation bearings: a literature review', *Earthquake spectra* **8**(2), 279–303.
- Tiersten, H. (1971), 'On the nonlinear equations of thermo-electroelasticity', *International Journal of Engineering Science* **9**(7), 587–604.
- Toupin, R. A. (1956), 'The elastic dielectric', *Journal of Rational Mechanics and Analysis* **5**(6), 849–915.
- Treloar, L. R. G. (1975), *The physics of rubber elasticity*, Oxford University Press, USA.
- Tsai, Y. M. and Kolsky, H. (1968), 'Surface wave propagation for linear viscoelastic solids', *Journal of the Mechanics and Physics of Solids* **16**(2), 99–100.
- Vellekoop, M. J. (1998), 'Acoustic wave sensors and their technology', *Ultrasonics* **36**(1-5), 7–14.
- Wan, X., Tse, P., Xu, G., Tao, T. and Zhang, Q. (2016), 'Analytical and numerical studies of approximate phase velocity matching based nonlinear s0 mode lamb waves for the detection of evenly distributed microstructural changes', *Smart Materials and Structures* **25**(4), 045023.
- Wang, H., Lei, M. and Cai, S. (2013), 'Viscoelastic deformation of a dielectric elastomer membrane subject to electromechanical loads', *Journal of Applied Physics* **113**(21), 213508.
- Wang, M. C. and Guth, E. (1952), 'Statistical theory of networks of non-gaussian flexible chains', *The Journal of Chemical Physics* **20**(7), 1144–1157.
- Wang, Y., Xue, H., Chen, H. and Qiang, J. (2013), 'A dynamic visco-hyperelastic model of dielectric elastomers and their energy dissipation characteristics', *Applied Physics A* **112**(2), 339–347.
- Wei, K., Domicone, N. W. and Zhao, Y. (2014), 'Electroactive liquid lens driven by an annular membrane', *Optics letters* **39**(5), 1318–1321.

- Wissler, M. and Mazza, E. (2005), 'Modeling and simulation of dielectric elastomer actuators', *Smart Materials and structures* **14**(6), 1396.
- Wissler, M. and Mazza, E. (2007), 'Mechanical behavior of an acrylic elastomer used in dielectric elastomer actuators', *Sensors and Actuators A: Physical* **134**(2), 494–504.
- Worlton, D. (1961), 'Experimental confirmation of lamb waves at megacycle frequencies', *Journal of Applied Physics* **32**(6), 967–971.
- Xu, P.-c. and Bar-Cohen, Y. (1990), 'Leaky lamb waves for the ultrasonic nondestructive evaluation of adhesive bonds', *Journal of Engineering Materials and Technology* **112**, 255.
- Yang, E., Frecker, M. and Mockensturm, E. (2005), Viscoelastic model of dielectric elastomer membranes, in 'Smart Structures and Materials 2005: Electroactive Polymer Actuators and Devices (EAPAD)', Vol. 5759, International Society for Optics and Photonics, pp. 82–94.
- Yeoh, O. H. (1993), 'Some forms of the strain energy function for rubber', *Rubber Chemistry and technology* **66**(5), 754–771.
- Yong, H., He, X. and Zhou, Y. (2011), 'Dynamics of a thick-walled dielectric elastomer spherical shell', *International Journal of Engineering Science* **49**(8), 792–800.
- Yun, S., Park, S., Nam, S., Park, B., Park, S. K., Mun, S., Lim, J. M. and Kyung, K.-U. (2016), 'An electro-active polymer based lens module for dynamically varying focal system', *Applied Physics Letters* **109**(14), 141908.
- Yun, S., Park, S., Park, B., Nam, S., Park, S. K. and Kyung, K.-U. (2015), 'A thin film active-lens with translational control for dynamically programmable optical zoom', *Applied Physics Letters* **107**(8), 081907.
- Zhang, G., Gaspar, J., Chu, V. and Conde, J. (2005), 'Electrostatically actuated polymer microresonators', *Applied Physics Letters* **87**(10), 104104.

- Zhang, J., Chen, H., Li, B., McCoul, D. and Pei, Q. (2015), 'Coupled nonlinear oscillation and stability evolution of viscoelastic dielectric elastomers', *Soft Matter* **11**(38), 7483–7493.
- Zhang, X., Wissler, M., Jaehne, B., Breonmann, R. and Kovacs, G. (2004), Effects of crosslinking, prestrain, and dielectric filler on the electromechanical response of a new silicone and comparison with acrylic elastomer, in 'Smart Structures and Materials 2004: Electroactive Polymer Actuators and Devices (EAPAD)', Vol. 5385, International Society for Optics and Photonics, pp. 78–86.
- Zhao, X., Hong, W. and Suo, Z. (2007), 'Electromechanical hysteresis and coexistent states in dielectric elastomers', *Physical review B* **76**(13), 134113.
- Zhao, X. and Suo, Z. (2007), 'Method to analyze electromechanical stability of dielectric elastomers', *Applied Physics Letters* **91**(6), 061921.
- Zhao, X. and Suo, Z. (2008), 'Method to analyze programmable deformation of dielectric elastomer layers', *Applied Physics Letters* **93**(25), 251902.
- Zhao, X. and Suo, Z. (2010), 'Theory of dielectric elastomers capable of giant deformation of actuation', *Physical review letters* **104**(17), 178302.
- Zhou, J., Hong, W., Zhao, X., Zhang, Z. and Suo, Z. (2008), 'Propagation of instability in dielectric elastomers', *International Journal of Solids and Structures* **45**(13), 3739–3750.
- Zhou, J., Jiang, L. and Khayat, R. (2016a), 'Analysis on the energy harvesting cycle of dielectric elastomer generators for performance improvement', *EPL (Europhysics Letters)* **115**(2), 27003.
- Zhou, J., Jiang, L. and Khayat, R. E. (2014), 'Viscoelastic effects on frequency tuning of a dielectric elastomer membrane resonator', *Journal of Applied Physics* **115**(12), 124106.
- Zhou, J., Jiang, L. and Khayat, R. E. (2015), 'Investigation on the performance of a viscoelastic dielectric elastomer membrane generator', *Soft Matter* **11**(15), 2983–2992.

- Zhou, J., Jiang, L. and Khayat, R. E. (2016b), 'Dynamic analysis of a tunable viscoelastic dielectric elastomer oscillator under external excitation', *Smart Materials and Structures* **25**(2), 025005.
- Zhou, J., Jiang, L. and Khayat, R. E. (2017), 'Methods to improve harvested energy and conversion efficiency of viscoelastic dielectric elastomer generators', *Journal of Applied Physics* **121**(18), 184102.
- Zhu, Hristiyan Stoyanov, G. K. and Suo, Z. (2010), 'Large deformation and electromechanical instability of a dielectric elastomer tube actuator', *Journal of Applied Physics* **108**(7), 074113.
- Zhu, J., Cai, S. and Suo, Z. (2010a), 'Nonlinear oscillation of a dielectric elastomer balloon', *Polymer International* **59**(3), 378–383.
- Zhu, J., Cai, S. and Suo, Z. (2010b), 'Resonant behavior of a membrane of a dielectric elastomer', *International Journal of Solids and Structures* **47**(24), 3254–3262.
- Ziser, Y. and Shmuel, G. (2017), 'Experimental slowing of flexural waves in dielectric elastomer films by voltage', *Mechanics Research Communications* **85**, 64–68.

Curriculum Vitae

Name: Mohammad Mahdi Sheikh Bagher Mohajer

Post-Secondary Sharif University of Technology

Education and Tehran, Iran

Degrees: 2014 - 2017 Master of Engineering Science

University of Western Ontario

London, ON

2018 - 2020 Master of Engineering Science

Honours and Western Graduate Research Scholarship

Awards: 2018-2020

Related Work Teaching Assistant/Research Assistant

Experience: The University of Western Ontario

2018 - 2020